DUPLO Deliverable D3.2

Enhanced Solutions for Full-Duplex Transceivers and Systems

Project Number:	**316369**
Project Title	**Full-Duplex Radios for Local Access – DUPLO**
Deliverable Type:	**PU**

Contractual Date of Delivery:	**April 30, 2015**
Actual Date of Delivery:	**June 8, 2015**
Editor(s):	**Mir Ghoraishi (UniS)**
Author(s):	**Mir Ghoraishi, Dandan Liang, Gaojie Chen (UniS); Kari Rikkinen, Visa Tapio (UOulu).**
Work package:	**WP3**
Estimated person months:	**20**
Security:	**PU**
Nature:	**Report**
Version:	**1.0**

Abstract:

To enable full-duplex communications potential and gains in wireless networks, a first step is to design and implement full-duplex transceivers capable to overcome self-interference challenge inherent in full-duplex operation in various scenarios and setups. The DUPLO project aims to propose solutions for practical full-duplex transceivers and to introduce scenarios in which full-duplex operation can deliver system level gains. This work package, i.e. DUPLO WP3, is concerned with the digital baseband solutions for full-duplex transceivers. The full-duplex transceiver is designed to cancel the self-interference, i.e. the coupling of the transmit signal to the collocated receiver, as much as possible in the receiver RF and analog chain. None the less the residual self-interference remaining in the received signal at the digital baseband is a main concern in providing the high performance digital baseband solutions for the scenarios of interest, so that novel techniques at the full-duplex transceiver digital baseband are required to achieve the best performance of the system in various scenarios.

This deliverable investigates advanced solutions for the full-duplex digital baseband. Since a major concern in the design of a full-duplex radio is how to deal with the nonlinear components of the self-interference which is created due to the operation of system components with a nonlinear response. Specifically, since the transmitter PA has been identified as a main source of nonlinear components in the full-duplex system self-interference, the modelling, simulation and evaluation of the effect of PA on the performance of a full-duplex system is presented. In this regard, three different methods in the analysis of the problem is presented and performances are compared.

Moreover to evaluate the potential of the full-duplex operation for different scenarios, detection and multiple access schemes in a full-duplex system are analysed. In this regard different detection methods, namely zero-forcing, maximum likelihood and minimum mean square method, are analysed and the performances are comparatively evaluated through simulations. Simple multiple-access techniques in a multiuser full-duplex scenario are investigated as well.

MIMO is one of the most important techniques in the current wireless systems therefore full-duplex operation needs to coexist with this technology. A main challenge for full-duplex MIMO systems is how to cancel self-interference from multiple collocated transmit antenna concurrently, while preventing the LNA and ADC of the receive chain from saturation. However digital techniques, such as by precoding of the transmit signal, can help in mitigating this effect. A couple of precoding techniques are introduced and the performances are examined.

One of the DUPLO projects targets is to demonstrate the integrated solutions for full-duplex transceivers. In this regard the practical digital baseband algorithms to be used in the DUPLO proof-of-concept are designed and implemented on the hardware. These work in cooperation with antenna, isolation circuits and active RF cancellation circuits to provide the full proof-of-concept for the DUPLO solutions. The performance of the employed algorithm with different RF solutions are examined and presented.

Keyword list: full-duplex, digital baseband, self-interference cancellation, self-interference channel, channel estimation, digital self-interference cancellation, power amplifier nonlinear model, detection, multiple-access, full-duplex multiple-input multiple-output (MIMO), full-duplex relay link, full-duplex transceiver proof-of-concept

Executive Summary

This deliverable investigates 'enhanced digital baseband solutions for full-duplex transceiver'. In a previous deliverable, self-interference cancellation at digital baseband digital reported [1]. In that document, basic concepts in digital self-interference cancellation such as self-interference channel analysis and modelling and its estimation methods were presented. Moreover the limitations of antenna, RF and analog self-interference cancellation solutions introduced, and specifically their narrowband performance discussed. To achieve a wideband full-duplex system with good self-interference cancellation, a subband approach introduced, which cancels the wideband self-interference in several subbands, and its performance was simulated. Moreover the nonlinear components in the self-interference due to nonlinear components in the RF chains, such as PA, ADC and AGC, were introduced and preliminary discussions on the modelling and analysis of these effects were discussed.

In the current deliverable, more advanced digital solutions for self-interference cancellation in full-duplex systems are discussed and potential improvements are introduced. Moreover the digital self-interference solutions for the full-duplex system proof-of-concept are designed and evaluated.

Specifically, since the transmitter PA has been identified as a main source of nonlinear components in the full-duplex system self-interference, the modelling, simulation and evaluation of the effect of PA on the performance of a full-duplex system is presented. In this regard, three different methods in the analysis of the problem are presented and performances are compared.

Moreover different detection methods, namely zero-forcing, maximum likelihood and minimum mean square method, are analysed and the performances are comparatively evaluated through simulations. Simple multiple-access techniques in a multiuser full-duplex scenario are investigated as well.

Since MIMO is one of the most important techniques in the current wireless systems, full-duplex needs to coexist with this technology. A main challenge for full-duplex MIMO systems is how to cancel self-interference from multiple collocated transmit antenna concurrently, while preventing the LNA and ADC of the receive chain from saturation. At the digital baseband however smart precoding techniques can help in reducing the self-interference while maximizing the transmitted signal in the direction of the remote receiver. A couple of precoding techniques are introduced and the performances are examined when no digital self-interference cancellation is used (to evaluate the isolated effect on these precoding on the performance of the system). Then these precoding schemes are used with the digital self-interference cancellation assuming there can be an error in the self-interference channel estimation. The investigations shows that these precoding schemes, i.e. ZF and SLNR-based, can significantly improve the performance of a full-duplex MIMO system. On the other hand, achievable capacities in a point-to-point full-duplex MIMO link and a full-duplex MIMO relay link are investigated and compared to the half-duplex capacities. Results show that the full-duplex gain is achieved conditioned on a very good self-interference cancellation performance.

Finally, as input to the DUPLO proof-of-concept, practical digital self-interference cancellation algorithms are implemented which works in cooperation with antenna, isolation circuits and active RF cancellation circuits to provide the full proof-of-concept for the DUPLO solutions. These algorithms and their performances are discussed as well. The performance of the employed channel estimation technique is evaluated by using measured data. As well performances of digital self-interference cancellation in time domain and in frequency domain, using measured data from a full-duplex scenario measurement using antenna and RF self-interference cancellation are analysed and results are presented.

Authors

Partner	**Name**	**Email**
University of Oulu (**UOulu**)	Visa Tapio	Visa.tapio@ee.oulu.fi
	Kari Rikkinen	Kari.rikkinen@ee.oulu.fi
University of Surrey (**UniS**)	Mir Ghoraishi	m.ghoraishi@surrey.ac.uk
	Dandan Liang	d.liang@surrey.ac.uk
	Gaojie Chen	Gaojie.chen@surrey.ac.uk

Table of Contents

Abbreviations

ADC	analog to digital converter
AGC	automatic gain controller
AWGN	additive White Gaussian Noise
BER	bit error rate
BPSK	binary phase shift keying
CSI	channel state information
DAC	digital to analog converter
DFT	digital Fourier transform
DUPLO	full-DUPlex radios for LOcal access
IDFT	inverse digital Fourier transform
LNA	low noise amplifier
LS	least squares
LTE	long term evolution
LTS	long training sequence
MIMO	multiple-input multiple-output
ML	maximum likelihood
MMSE	minimum mean square error
OFDM	orthogonal frequency division multiplexing
OFDMA	orthogonal frequency-division multiple access
PA	power amplifier
PAPR	peak to average power ratio
QAM	quadrature amplitude modulation
SC-FDMA	single-carrier frequency-division multiple access
SINR	signal to interference-plus-noise ratio
SLNR	signal to leakage-plus-noise ratio
STS	short training sequence
SVD	singular value decomposition
ZF	zero forcing

1. Introduction

The DUPLO project aims at developing new technology and system solutions for future generations of mobile data networks by introducing a new full-duplex radio transmission paradigm, the same carrier frequency is used for transmission and reception at the same time. This 'full-duplex' approach holds the potential to significantly increase the capacity and spectrum usage. The main challenge for the full-duplex transceiver is to cancel the self-interference due to the transmit signal couplings to the collocated receiver. In practice, the achievable self-interference cancellation capability is limited, and also depended on multiple system constrains such as the form factors of the wireless devices. Therefore, potential applications of the full-duplex communications are also constrained by the achievable performance of practical full-duplex transceivers. Relevant scenarios and network architectures have been discussed in [2].

Self-interference cancellation is done mainly at the antenna (isolation), RF and analog circuits to keep the LNA and ADC from saturation and to minimize the noise elevation. Full-duplex transceiver at digital baseband is required to remove the residual self-interference which could not be removed by previous cancellations. The received signal at the digital baseband of the full-duplex transceiver includes residual of the linear self-interference, after analog/RF cancellation, and nonlinear components which are added to the signal in the transmitter and the receiver by nonlinear elements, e.g. power amplifier, mixers, LNA, etc. Therefore two main tasks expected from the full-duplex digital baseband are cancelling the residual self-interference and compensating nonlinear components. It is observed that digital cancellation in a full-duplex transceiver has the same structure as a general echo canceller.

In a previous deliverable [1], the analysis of self-interference channel which is a prerequisite for any baseband analysis and solution was discussed. Moreover a novel method for estimating the self-interference channel and the desired signal channel at the same time was proposed. In addition, limitations of digital baseband self-interference cancellation in a full-duplex transceiver were analyzed, among these the influence of multipath in self-interference channel and frequency selective isolation of transmit-receive path in the full-duplex transceiver were analyzed. A proposed scheme is presented in which the digital algorithm estimates the frequency selective self-interference channel, the nonuniform transmit-receive path isolation included, which jointly works with the RF self-interference cancellation circuit to improve the overall performance of the full-duplex system. This technique divides the received signal into several subbands (with equal bandwidths) and applies the self-interference cancellation on the subband signals. Nonlinear response of the transceiver components is another issue which was analyzed in the previous deliverable. The limitations by ADC and AGC settings on the full-duplex transceiver performance were investigated. As well the nonlinear components and effects in the full-duplex transceiver were modelled and analyzed [1]. These included nonlinearities due to power amplifier, IQ imbalance and phase-noise.

Since at the digital baseband, the transmit signal, functioning as the self-interference is known and the self-interference channel can be estimated at the collocated receiver, in principle the interference cancellation can be done by just subtracting the emulated self-interference, using the transmit signal and the self-interference channel estimate, the received signal. However usually the cancellation performance is not as expected, sue to nonlinear effects in the in the self-interference path which distort the signal, i.e. linear digital processing alone cannot reproduce and cancel the self-interference accurately enough. This means that advanced modelling and processing, taking into account the different analog impairments, is required in order to produce a sufficiently accurate cancellation signal. For instance, modelling nonlinear distortion in the digital SI regeneration and cancellation has been shown to improve the performance of a practical

in-band full-duplex transceiver [3]. In the previous deliverable the full-duplex transceiver nonlinear effects on the self-interference cancellation, specifically effects due to PA, IQ imbalance and phase-noise, were analysed. The effects of uncorrelated phase noise of the transmitter and receiver oscillators has been analysed in recent literature as well, e.g., in [4],[5]. In these studies it was observed that the phase noise can potentially limit the amount of achievable SI suppression, especially when using two separate oscillators for transmitter and receiver. Furthermore the impact of IQ was analysed in [6]. On the other hand, our analyses as well as those presented in [7] indicate that PA is the source of significant nonlinear components in the full-duplex transceiver self-interference. A nonlinear digital self-interference cancellation to handle both linear and nonlinear self-interference simultaneously was proposed in [8]. In section 2, three different approaches in baseband self-interference cancellation are investigated. First, linear self-interference channel estimation is used to reconstruct the self-interference, to be used for self-interference cancellation. In the second approach and in the training, first the linear estimate of the self-interference channel is used to remove the linear self-interference from the received signal and then the remaining signal is used to estimate the remaining nonlinear component by an LS estimator. Finally, in the third approach nonlinear amplifier model and linear self-interference model are used simultaneously as a Hammerstein model, and then the parameters are estimated using the LS estimator. The performance of each approach is discussed comparatively.

Data detection and multiple access schemes for full-duplex systems are important issues to be addressed in order to design a full-duplex system with the optimum performance and maximum capacity. If the full-duplex system can totally cancel the self-interference, there is no extra considerations in in a full-duplex system when using the half-duplex data detection and multiple access schemes. However no full-duplex transceiver works perfectly in self-interference cancellation and it is safe to assume that there is a residual self-interference remained in the system after all cancellations in different levels. A good multiple access scheme should maximize the capacity of a wireless network, i.e., the number of admissible users for a given available total bandwidth and a proper detection scheme should strike the balance between performance and complexity based on the system quality of service requirement. Section 3 of this deliverable reports the investigations on the performance of two main multiple access used in the LTE systems, i.e. OFDMA and SC-FDMA. The multiple access schemes are evaluated using three popular detection schemes, i.e. zero-forcing (ZF), maximum likelihood (ML) based and minimum mean square error (MMSE) detection schemes are employed. The analysis and simulation results are presented in section 3.

One important barrier in popularizing full-duplex technology is about its operation and coexistence with MIMO technology. It is known that achieving spatial gain of the wireless channel by using multiple antenna techniques in MIMO systems is one of the most important breakthroughs in wireless technology during the last couple of decades [9]. However how the full-duplex scheme, more specifically self-interference cancellation techniques, can be adopted in MIMO systems is not straightforward. On the other hand it is well conceived that if full-duplex is going to be widely deployed, it needs to work well in MIMO systems. To gain a better understanding of the performance of full-duplex MIMO systems under practical constraints, the work presented in [10] derives achievable rate bounds using a realistic system model, including channel estimation errors and effects of limited dynamic range. It is shown that the full-duplex MIMO spectral efficiency is uniformly better than its optimized half-duplex counterpart and nearly double when operating within dynamic range constraints. One of the first works on full-dulex MIMO system requires 4M antennas for building a full-duplex M antenna MIMO radio, and even then fails to provide the needed self-interference cancellation for WiFi systems (20 MHz bandwidth) to achieve the expected doubling of throughput [11]. A more practical method to overcome the self-interference cancellation challenge between all full-duplex MIMO transceiver

chains is proposed in [12]. When a full duplex MIMO radio transmits, the transmission from any one of the M antennas (interchangeably referred to as transceiver chains) propagates to the other antenna (chains) and causes a large amount of interference. In this work, instead of introducing a separate copy of the cancellation circuit for each pair of MIMO transceiver chains, and DSP algorithm for each pair of chains that experiences the so called cross-talk, only one cancellation circuit per receive chain is used. Here it is assumed that MIMO chains are collocated and share similar environment, so that the self-interference channel from all transmit chains to each receive chain are common. Moreover a method to estimate self-interference channels from all transmit chains to each receive chains concurrently is used which improves the overall performance which otherwise would degrade linearly with the number of MIMO antennas at each link end. This work is prototyped and performance of the proposed schemes is evaluated using off-the-shelf radios and test equipment [12]. The remaining question is if the assumed common channel for the M transmit-chains to each receive chain is always a good estimate of the MIMO self-interference channels. Moreover the self-interference cancellation using delay and attenuation in RF domain has its own limitation in recreation of long delays. Overall, self-interference cancellation for MIIMO systems is still needs careful consideration and novel approaches. Moreover, to improve the confidence, these solutions needs to be implemented on the real transceivers and the performance shall be compared to MIMO systems. Meanwhile digital solutions can help improving the overall the self-interference cancellation of the full-duplex MIMO systems. The topic of section 4 in the current deliverable is examining precoding schemes in gaining the residual self-interference cancellation at the full-duplex MIMO digital baseband. The analysis shows that on the top of self-interference cancellations at RF and analog circuits, digital solutions, such as precodings, can help to improve the system performance. The performance of these solutions, as those of their single antenna counterparts, depends on the accuracy of the MIMO self-interference channel estimation as well on how precise the nonlinear components in the self-interference are estimated and modelled.

Finally, section 5 presents the digital solutions for the full-duplex transceiver proof–of-concept. Particularly, the self-interference channel estimation, self-interference cancelation in time domain, and self-interference cancellation cancelation in frequency domain for the actual self-interference cancellation in the proof-of-concept are introduced and applied to the measurement data. The comparative analysis of the digital baseband cancellation is then presented in this section.

2. Self-interference cancellation methods when nonlinearity exists in the system

2.1. Motivation

As it was discussed in section 1, in order to fulfil high self-interference cancellation requirements, the nonlinear effects and components needs to be considered in the self-interference cancellation. The transmitter PA imposed strong nonlinear effects, which need to be estimated and cancelled properly. To this end the performance of using linear self-interference cancellation with and without nonlinear component modelling and cancellation are presented in this section followed by simulations based on measured self-interference channel values. The nonlinear operation of the PA is modelled with a commonly used Modified Saleh model.

2.2. System model

The system considered in this chapter is a single link between two nodes, i.e. local and remote nodes. The block diagram of each node is presented in Fig. 2.1. The baseband self-interference cancellation is performed using feed-forward principle. The estimated self-interference channel and known transmitted signal are used to form the emulated self-interference signal which is then subtracted from the received signal in order to cancel the self-interference as illustrated in Fig. 2.1.

Both nodes use OFDM for data transmission. In order to attain high self-interference cancellation performance at baseband the self-interference channel must be estimated accurately. If during the self-interference channel estimation the received signal is sum of self-interference and desired signal, the desired signal acts as interference for self-interference channel estimation. To guarantee the best possible self-interference channel estimation accuracy, the frame structure of Fig. 2.2 is assumed. At the beginning of the frame node 1 sends a preamble. This preamble is used at node 1 to estimate its self-interference channel and at node 0 to estimate the channel between nodes. Node 1 stops transmitting after it has sent the preamble and node 0 starts its transmission. Node 0 estimates its self-interference channel and node 1 estimates the channel between the nodes. After both nodes have estimated their self-interference channels and the channel between them, they can start data transmission in the full-duplex mode. This arrangement of preambles allows interference free self-interference channel estimation but at the same time increases the overhead. If the self-interference channel does not change during longer periods the increase in the overhead can be reduced by using a longer data frame. Thus the amount of overhead varies based on the pace of the self-interference channel variation, which itself depends on the scenario and the environment. The demonstrator developed in the DUPLO WP5 uses similar frame structure. This structure is described in detail in WP5 deliverable, D5.2 [13].

During the full-duplex transmission, the received signal can be expressed as

$$r(t) = h(t) * x(t) + h_{SI}(t) * x_{SI}(t) + n(t) \tag{2.1}$$

where $x(t)$ is the desired signal from a distant transmitter, $h(t)$ is the desired signal channel, $x_{SI}(t)$ is the self-interference signal (i.e. local node's transmitted signal), $h_{SI}(t)$ is the self-interference channel and $n(t)$ is the noise term. The symbol $*$ indicates convolution operation.

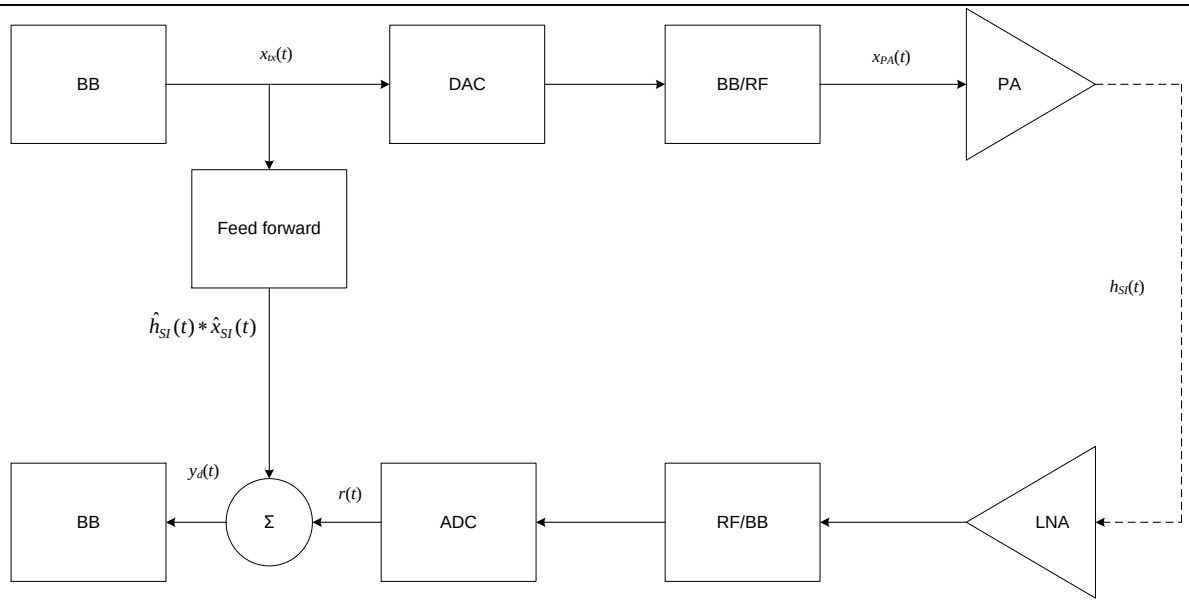

Fig. 2.1. Baseband self-interference cancellation in full-duplex transceiver.

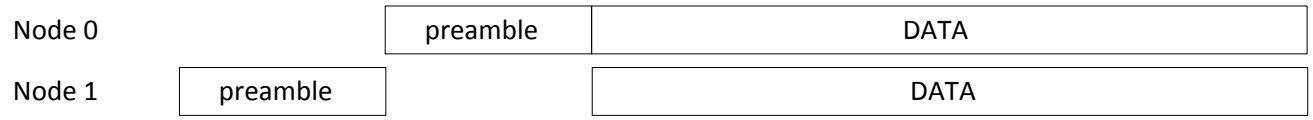

Fig. 2.2. Full-duplex communication frame structure.

2.3. PA model

The nonlinear power amplifier is modeled using the Modified Saleh - I (MS-I) model, which models amplitude (AM-AM) and phase (AM-PM) distortions of a memoryless solid state power amplifier [14]. AM-AM and AM-PM distortions are given as [14]

$$g[r(t)] = \frac{\alpha_{\text{am}} r(t)}{\sqrt{1+\beta r(t)^3}} \tag{2.2}$$

$$\Phi[r(t)] = \frac{\alpha_{\text{pm}}}{\sqrt[3]{1+r(t)^4}} - \varepsilon \tag{2.3}$$

where $r(t)$ is the envelope of the PA input signal. Parameter values are used to match the model with measured amplifier response curves. Parameter values used in this work are $\alpha_{\text{pm}} = 0.161$, $\alpha_{\text{am}} = 1.0536$, $\beta = 0.08594$ and $\varepsilon = 7.1$ degrees [14]. AM-AM and AM-PM curves with these parameters are shown in Fig 2.3.

In the simulations the amplifier has been driven with three different back-off values. Here the back-off is defined as power difference between the PA saturation level and the maximum value of the output signal. These different back-off values correspond with different levels of nonlinearity. A common measure for amplifier nonlinearity is the third order intermodulation

distortion (IMD_3) which is defined as the power difference of a fundamental tone and third order distortion product in a two tone test (see e.g. [15]). Fig. 2.4 illustrates the signals used in two-tone test. With the used model the back-off values 1 dB, 3 dB and 6 dB correspond to IMD_3 values -24.1 dB, -31.1 dB and -40.1 dB respectively.

The SI channel model is obtained from measurements on the electrical balance based analog self-interference cancellation technique developed in DUPLO WP2 and described in [16], [17]. The frequency response of the measured self-interference channel is presented in Fig. 2.5. The attenuation of the assumed analog cancellation averaged over the whole frequency band of the OFDM signal is 46 dB with maximum cancellation value of 81.8 dB.

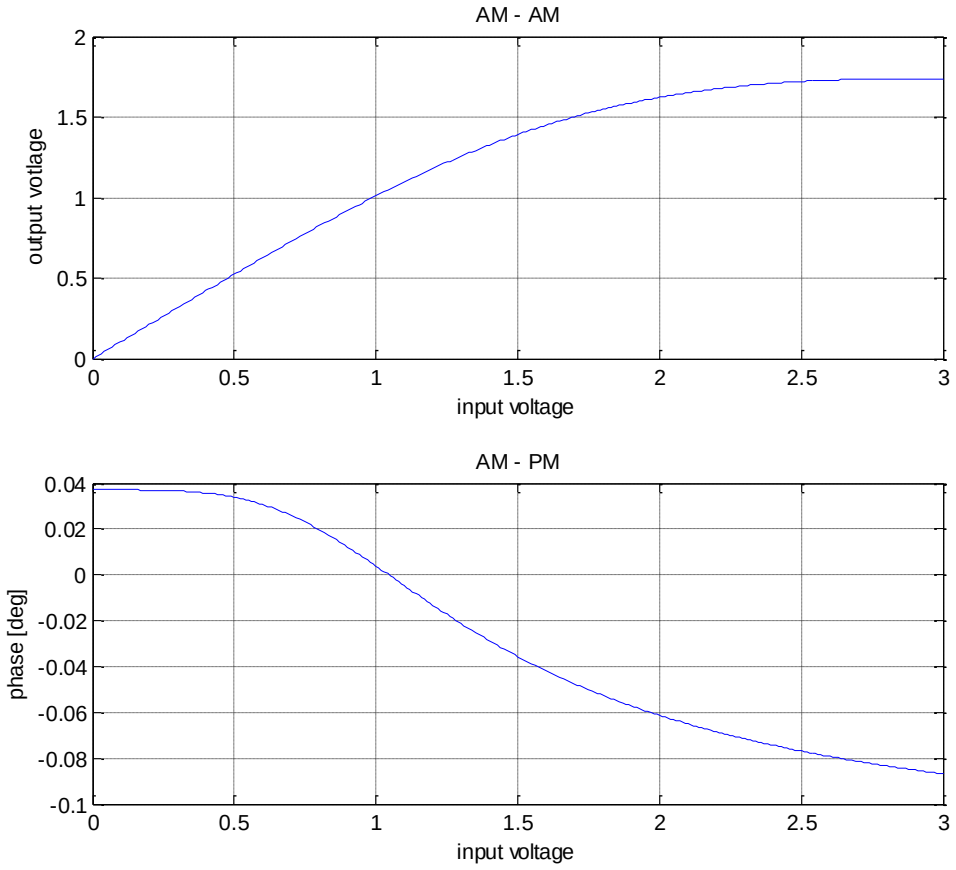

Fig. 2.3. Power amplifier model's amplitude and phase response.

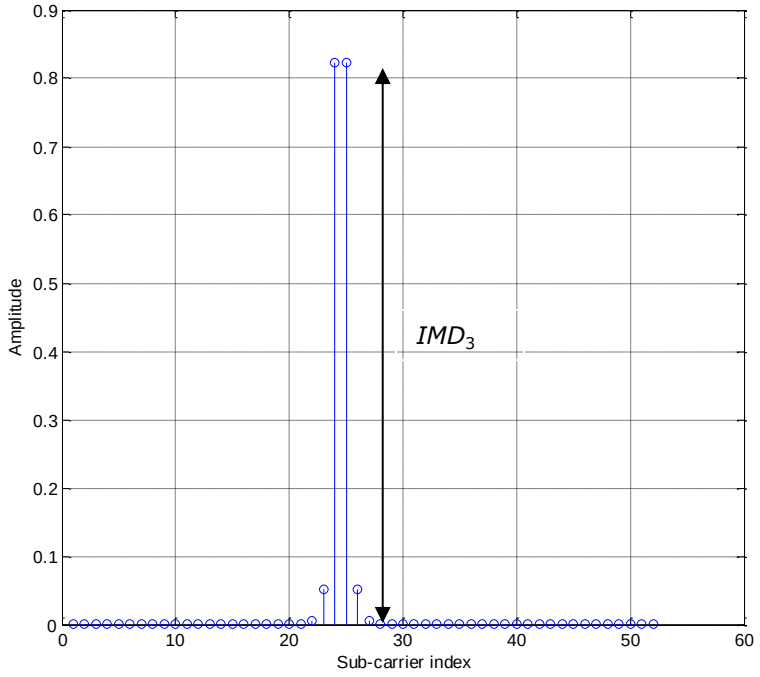

Fig. 2.4. Power amplifier two-tone test.

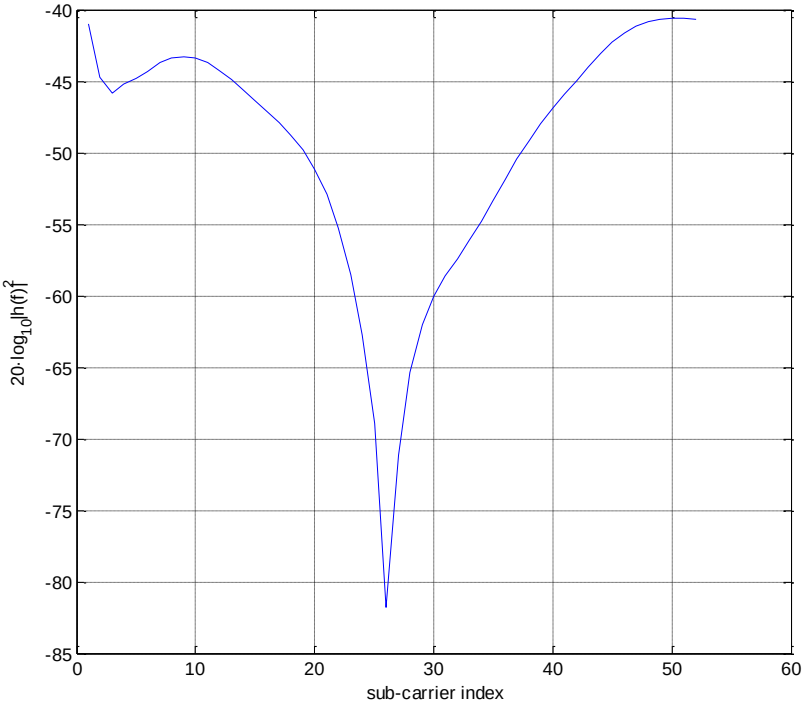

Fig. 2.5. Frequency response of the measured self-interference channel.

2.4. Self-interference cancellation

Three different baseband self-interference cancellation methods are considered. The simplest method is to use linear channel estimation for the creation of the cancellation signal. In the

second method, the self-interference channel estimation is done in two steps. In the first step, the channel is estimated using linear self-interference channel estimation. This channel estimate is then used to equalize the nonlinearity estimation training signal. Using the equalized training signal the nonlinearity is estimated using least squares (LS) estimator. In the third method the cascade of the nonlinear amplifier and linear self-interference channel are modeled as a Hammerstein model and model parameters are estimated using a LS estimator.

2.4.1. Linear self-interference cancellation

The simplest method for the self-interference cancellation is to use the same channel estimator for self-interference channel estimation that is used in the reception of the desired signal. When using the IEEE 802.11 standard, the preamble used for linear self-interference cancellation is the long training sequence (LTS) [18]. The channel estimate at subcarrier k is [19]

$$\hat{h}_k = \frac{1}{2}\left(r_{1,k} + r_{2,k}\right)x_k^* \tag{2.4}$$

where $r_{i,k}$ is the received sample at subcarrier k during the reception of i^{th} symbol of the preamble, x_k is the k^{th} element of the long training sequence. In 802.11 standard two identical LTS symbols are sent during preamble transmission.

2.4.2. Two-step method

With linear cancellation, the effect of the PA nonlinearity is omitted. A straightforward extension of the linear cancellation is to add a specific training sequence to the preamble for PA nonlinearity estimation. Training sequence consists of sample values that cover the whole dynamic range of the transmitted signal. The channel is first estimated using the same estimator as in the linear cancellation case. This self-interference channel estimate is then used to equalize the PA training sequence. After this, the PA nonlinearity is estimated using the equalized training sequence. The PA response estimation is based on the usage of polynomial functions to mimic the power amplifier operation. When the transmitter's known data signal before nonlinearity is x_{tx}, the PA response is modeled as

$$\hat{x}_{\text{SI}} = \sum_p c_p x_{\text{tx}}^p \tag{2.5}$$

Least squares estimate for coefficients in vector format ($\mathbf{c}=[c_0\, c_1 \ldots c_{\text{P}}]^{\text{T}}$) is

$$\mathbf{c} = \left(\mathbf{G}^{\text{H}}\mathbf{G}\right)^{-1}\mathbf{G}^{\text{H}}\mathbf{x}_{\text{SI}}^{\text{test}} \tag{2.6}$$

where $\mathbf{x}_{\text{SI}}^{\text{test}}$ is a vector whose elements are samples of the equalized PA training sequence and matrix $\mathbf{G}$ elements are calculated from known PA training sequence $\text{g}=g_1, g_2, \ldots g_P$, i.e, during the training sequence transmission the signal $x_{\text{tx}} = \text{g}$. Matrix $\mathbf{G}$ is

$$G = \begin{bmatrix} 1 & g_1 & g_1^2 & g_1^3 & g_1^P \\ 1 & g_2 & g_2^2 & g_2^3 & g_2^P \\ 1 & g_3 & g_3^2 & g_3^3 & g_3^P \\ 1 & g_4 & g_4^2 & g_4^3 & g_3^P \\ \vdots & & & & \\ 1 & g_P & g_P^2 & g_P^3 & g_P^P \end{bmatrix} \tag{2.7}$$

2.4.3. Hammerstein model based self-interference cancellation

Hammerstein model is a cascade of static nonlinear part followed by a linear filter [14]. It is a commonly used method for modeling PAs with memory and a natural choice for modeling a cascade of a PA and frequency selective self-interference channel as illustrated in Fig. 2.6. The usage of the Hammerstein model in self-interference cancellation has been introduced in [8]. In this case the duplexer in Fig. 2.6 is the electrical balance based analog self-interference cancellation developed in DUPLO WP2.

The Hammerstein model for parametric identification of the nonlinear self-interference channel can be written as [14]

$$y_n = \sum_{p=1}^{P} \sum_{k=1}^{M} h_{p,k} g_p(x_{n-k}) \tag{2.8}$$

where $h_{p,k}$ are coefficients of the linear filter, $g_p(\cdot)$ are kernel functions used for modeling the nonlinear part, P is the used nonlinearity order and M is the length of the linear filter. Kernel functions used are

$$g_p(x_n) = x_n |x_n|^{p-1} \tag{2.9}$$

where x_n is the known transmitted signal. Filter coefficients $h_{p,k}$ are estimated using a LS estimator.

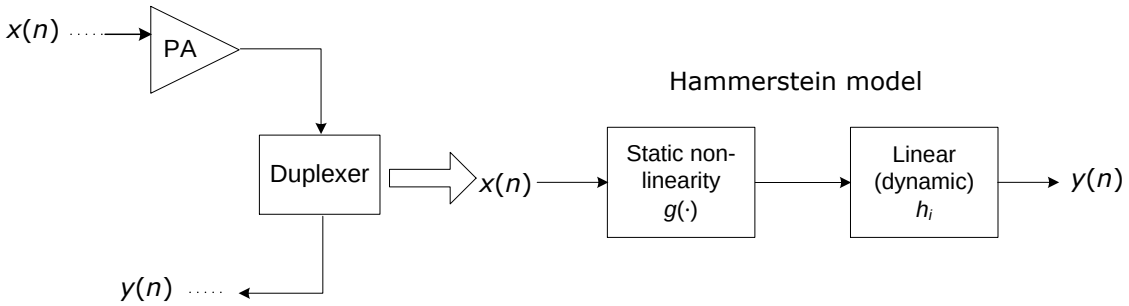

Fig: 2.6. Hammerstein model.

2.5. Simulations

The signal used in the simulations is an OFDM signal with 52 subcarriers[1]. The performances of the linear and two step SI cancellation methods in frequency flat and frequency selective channels are shown in Fig. 2.7 and 2.8, respectively. Solid lines show the performance of the linear cancellation and dashed lines the performance of the two-step method. The PA training sequence length *P* has been 5. Curves with asterisks, triangles and circles show the performances with 1 dB, 3 dB and 6 dB back-off. *INR* is the self-interference-to-noise ratio before the baseband cancellation. With the frequency flat self-interference channel the two-step method outperforms the linear method by 5 dB with high *INR*. The linear method has the same performance in both the frequency flat and frequency selective channel cases. However, the performance of the two

[1] Signals used in WP2 and WP5 are OFDM signals with 52 nonzero subcarriers.

step method is severely affected by the frequency selectivity. This implies that the performance of the used channel equalization is not sufficient. It can also be seen that at low INR values the linear method gives better performance than the two-step method. In the two-step method the nonlinearity is estimated using the equalized training sequence and at low INR values the error in the equalized training sequence limits the performance of nonlinearity estimation.

The performance of the self-interference cancellation using the Hammerstein model in the case of frequency selective self-interference channel is presented in Fig. 2.9 and 2.10. In the case of Fig. 2.9, the estimation is done using a data signal. In this approach the self-interference channel can be estimated while transmitting data to the distant node in the half-duplex mode and the full-duplex mode is started after both nodes have estimated their nonlinear self-interference channels, i.e., the preamble in Fig. 2.2 can be used to send useful information. Fig. 2.10 shows the performance when a preselected preamble is used. The fixed preamble is found with a computer search by testing different signals and selecting the one that gives the best performance with the fifth order nonlinearity model. Solid and dashed lines in figures 2.9 and 2.10 show the performance when the nonlinearity order of the Hammerstein model is P=3 and P=5 respectively. As can be seen the fifth order model gives significantly better performance than the third order model. The length of the preamble in all the cases has been 207 samples.

Self-interference cancellation performances shown in figures 2.9 and 2.10 are average values from 10,000 simulation iterations. The usage of a fixed preamble results in better self-interference cancellation compared to the self-interference cancellation with a random data signal as preamble. The computational cost is also lower with the preselected preamble than with the random one, since the matrix operations needed in the LS estimation of the filter coefficient estimation can be precomputed whereas the usage of random data for coefficient estimation requires matrix operations to be done during the data transmission. The benefit of the random preamble is that it allows data transmission in half-duplex mode while estimating the self-interference channel.

In nonlinear system identification, the used training signal can have a significant impact on the performance, e.g., the range of the self-interference cancellation values with the random preamble is between -51.1 dB and -21.2 dB and between -51.1 and -48.9 dB with fixed preamble when INR is 50 dB, PA back-off is 6 dB and Hammerstein model nonlinearity order is P=5. This shows that some realizations of the random preamble results in poor self-interference cancellation. However, in most of the cases both the preselected and random preamble gives similar performance as can be seen in figures 2.11 and 2.12. However, the usage of random data signal for nonlinear self-interference channel estimation can result in loss of some data frames due to failure in cancellation.

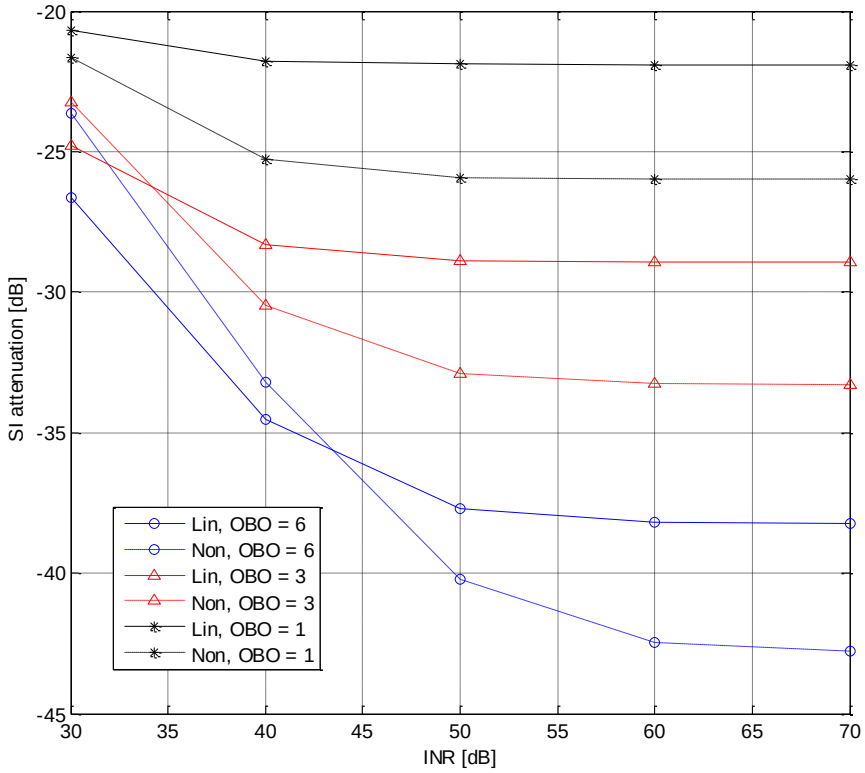

Fig.2.7. Performances of linear and two-step methods self-interference cancellation for a frequency flat self-interference channel.

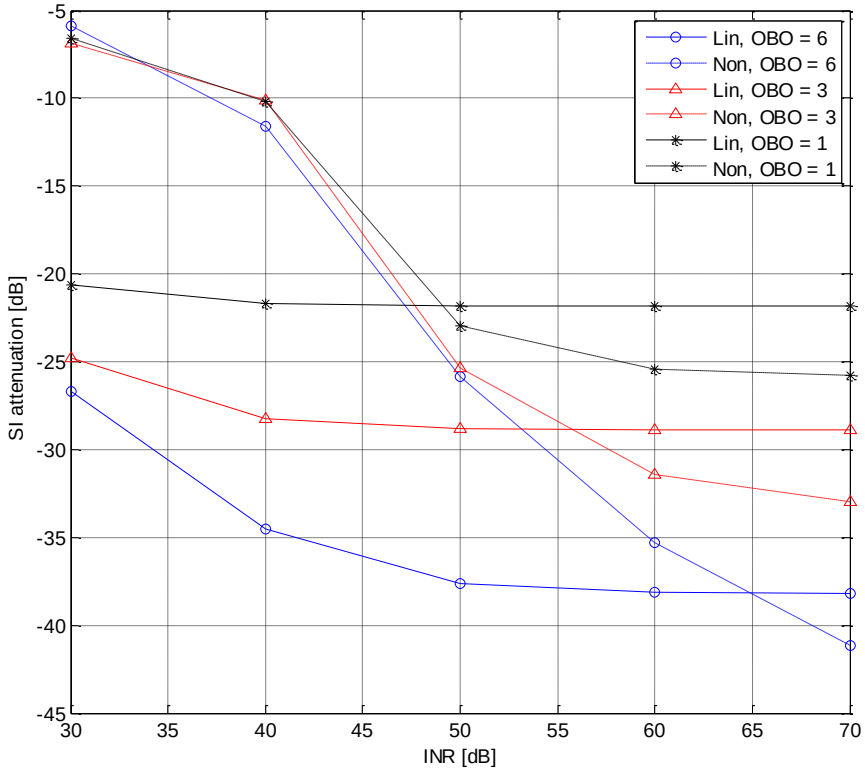

Fig. 2.8. Performances of linear and two-step method self-interference cancellation for a frequency selective self-interference channel.

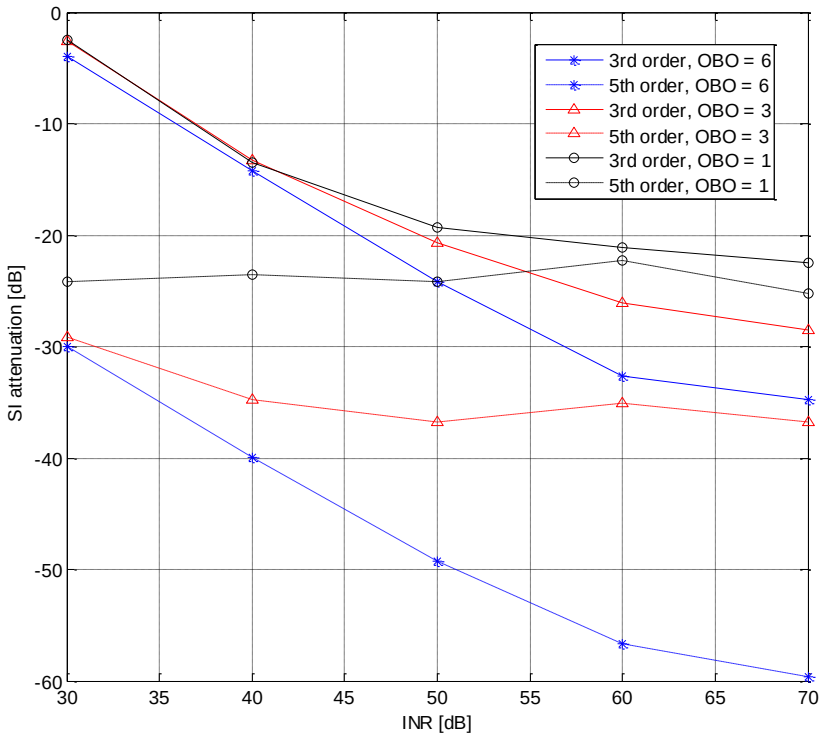

Fig.2.9. Hammerstein model based self-interference cancellation with random preamble.

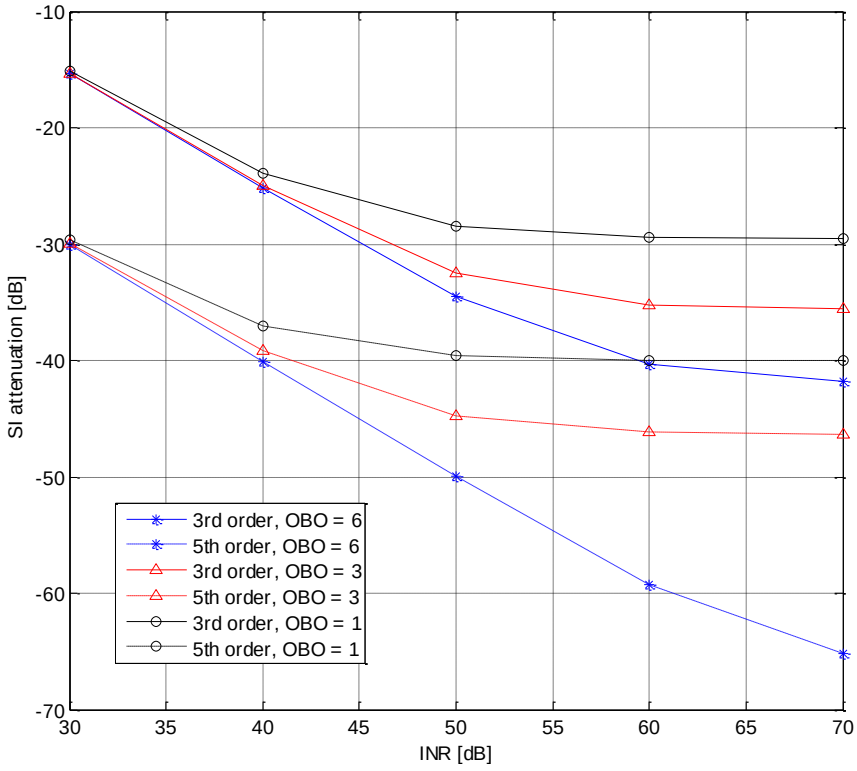

Fig. 2.10: Hammerstein model based self-interference cancellation with preselected preamble.

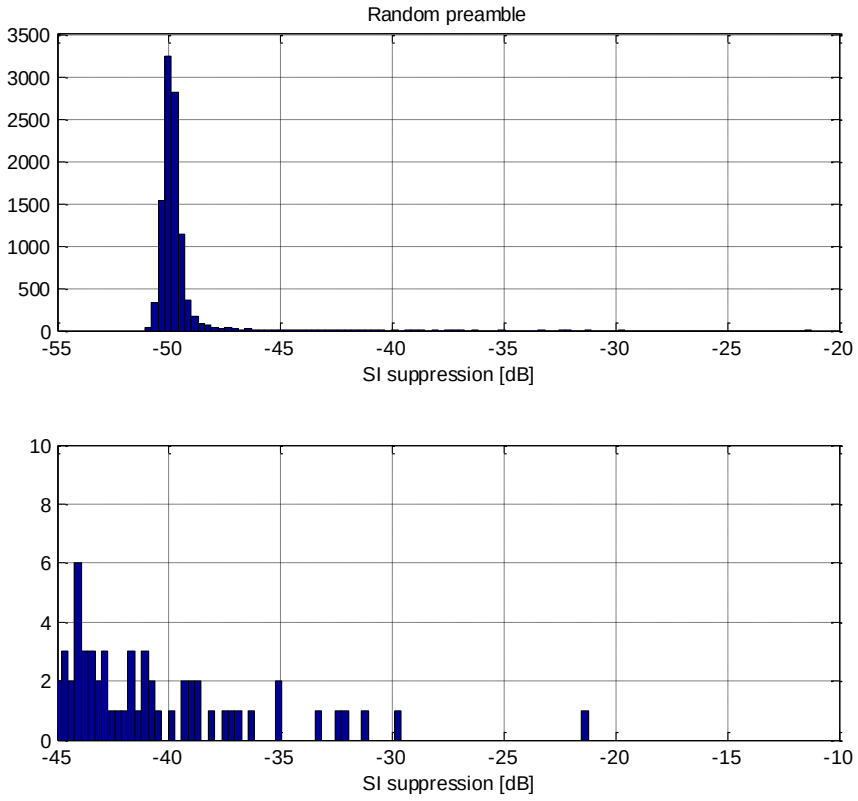

Fig. 2.11. Hammerstein based self-interference cancellation with random preamble, 5th order nonlinearity, OBO=6, INR=50 dB.

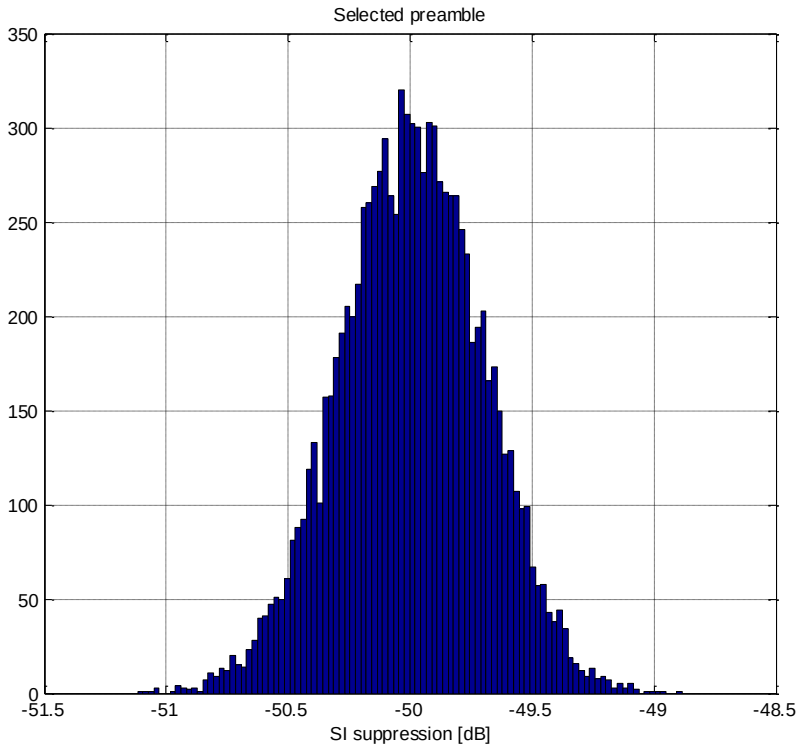

Fig.2.12. Hammerstein based self-interference cancellation with preselected preamble, 5th order nonlinearity, OBO=6 dB, INR=50 dB.

2.6. Summary

The analysis of the full-duplex systems shows that PA can cause nonlinear self-interference components which need to be modelled and cancelled. In this section, a cascade of nonlinear PA and frequency selective analog cancellation was considered. It was assumed that the receiver does not have knowledge on the form of the nonlinearity. Three self-interference cancellation methods were considered and comparatively analyzed. The linear method, which does not include any modelling of the PA, has only a minor effect on the complexity of a conventional transceiver's baseband processing. In this approach self-interference channel is estimated and used in reconstructing the received self-interference by using the knowledge of the transmit signal. Self-interference channel estimate needs an additional buffer and a path from the transmitter to the receiver chain is required. In addition, the same signal structure that is used in half-duplex systems can be used. The only modification to the frame structure is the timing of preambles and data signals to allow the self-interference channel estimation. By adding a short PA training sequence to frame, the PA nonlinearity can be compensated partly when the channel is frequency flat. But in the case of frequency selective self-interference channel performance improvement is smaller and requires higher self-interference levels than the linear method to work. The best performance is attained with the Hammerstein model based self-interference cancellation, but the problem with this method is the high computational complexity. The usage of a random preamble allows the system to transmit data in half-duplex mode while estimating the nonlinear self-interference channel, but can occasionally result in channel estimation failure. The best performance is attained with the Hammerstein based self-interference cancellation using fixed preamble. Also the processing power requirement of the self-interference channel estimation is lower with fixed preamble than with a random preamble. This is because the matrix operation which is required in the filter coefficient estimation can be precalculated.

3. Multiple-Access for Full-Duplex Systems

3.1. Motivation and system model

In this section, performance of multiple access schemes for a full-duplex system is investigated. Although it is assumed that self-interference cancellation and isolation at antenna, RF and digital baseband is employed, but there a residual self-interference is remained. The question is if this remaining residual self-interference affects the performance of the multiple access schemes and data detection algorithms in a different way from the half-duplex systems.

Here the performances of OFDMA and SC-FDMA schemes in a full-duplex system are investigated. OFDMA is a multiuser version of the OFDM digital modulation scheme which allows simultaneous low data rate transmission from several users. Multiple-access is achieved in OFDMA by assigning subsets of subcarriers to individual users [20]. Figure 3.1 shows the OFDMA system model where it is assumed that it operates in full-duplex. The transmit data goes through a serial-to-parallel, subcarrier mapping, IDFT, cyclic prefix insertion and pulse shaping, DAC and RF circuits and the transmit antenna. On the receive path the received data passes through the receive antenna, receive RF path, ADC, cyclic prefix removal, DFT, subcarrier demapping and equalization, and the parallel-to-serial.

Since OFDMA has a high PAPR, SC-FDMA, attributed with its low PAPR, is a good alternative for the uplink where lower PAPR greatly benefits the mobile terminal in terms of transmit power efficiency and low cost power amplifier [21]. SC-FDMA has been adopted as the multiple-access scheme for uplink in 3GPP Long Term Evolution (LTE). Figure 3.2 shows the system model of SC-FDMA. The differences between OFDMA and SC-FDMA are the added N-point DFT and parallel-to-serial at the SC-FDMA transmitter and the added N-point IDFT and serial-to-parallel at the SC-FDMA receiver.

Assuming there is multipath in the self-interference channel, it is reasonable to assume the residual self-interference as a random quantity with Rayleigh or Rician fading distribution. Thus a small-scale (flat) fading assumed which is remained approximately constant for (at least) one signalling interval. With this model of fading channel the main difference with respect to an AWGN channel resides in the fact that fading amplitudes are now Rayleigh or Rician distributed random variables, whose values affect the signal amplitude of the received signal.

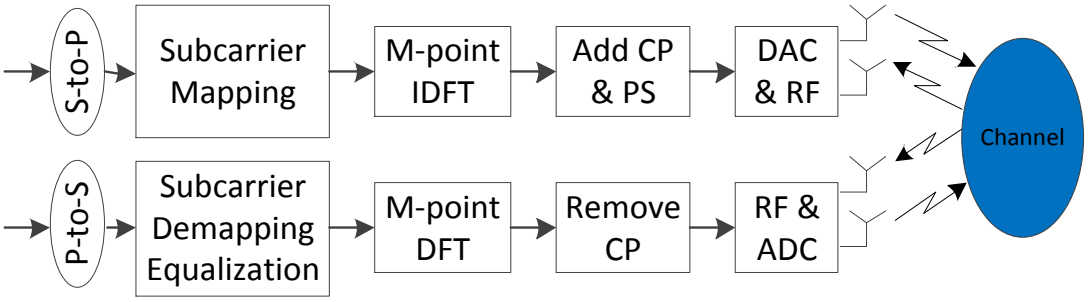

Figure 3.1. System model for OFDMA for full-duplex system.

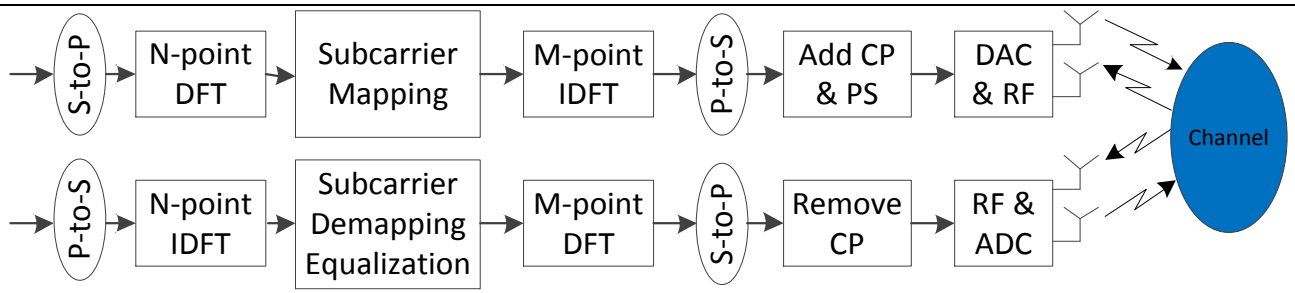

Figure 3.2. System model of SC-FDMA for full-duplex systems.

3.2. Detection schemes

3.2.1. Maximum likelihood detection scheme

The objective of the receiver is to obtain an estimate of the message, $\boldsymbol{s}$, from the given data in $\boldsymbol{y}$ with white Gaussian noise $\boldsymbol{n}$ and channel impulse response matrix H, where

$$\boldsymbol{y} = H\boldsymbol{s} + \boldsymbol{n}. \tag{3.1}$$

The ML detector minimizes the probability of error P_e can be obtained as

$$P_e \triangleq \mathrm{P}(\boldsymbol{s} \neq \tilde{\boldsymbol{s}}), \tag{3.2}$$

where $\mathrm{P}(.)$ denotes the probability function and $\tilde{\boldsymbol{s}}$ denotes the estimated symbol. Note that minimizing the probability of error is equivalent to maximizing the probability of correctly estimating $\boldsymbol{s}$, i.e.

$$\mathrm{P}(\boldsymbol{s} = \tilde{\boldsymbol{s}}|\boldsymbol{y}, H). \tag{3.3}$$

To derive the criterion function commonly used in the receiver note that the probability of Eq. (3.2) may alternatively be written as [22]

$$\mathrm{P}(\boldsymbol{s} = \tilde{\boldsymbol{s}}|\boldsymbol{y}, \mathrm{H}) = \frac{\mathrm{P}(\boldsymbol{s}=\tilde{\boldsymbol{s}}) f_{\boldsymbol{y}|\boldsymbol{s},H}(\boldsymbol{y}|\boldsymbol{s}=\tilde{\boldsymbol{s}},H)}{f_{\boldsymbol{y}|H}(\boldsymbol{y}|H)}, \tag{3.4}$$

where $\mathrm{f}_{\mathrm{y|H}}$ and $\mathrm{f}_{\mathrm{y|s,H}}$ are the conditional probability density functions of $\boldsymbol{y}$ given H and ($\boldsymbol{s}$, H), respectively. Because neither $\mathrm{P}(\mathrm{s} = \tilde{\mathrm{s}})$ nor $\mathrm{f}_{\mathrm{y|H}}(\boldsymbol{y}|H)$ depends on $\tilde{\mathrm{s}}$ the criterion of Eq. (3.2) is maximized by the $\tilde{\mathrm{s}}$ which maximizes

$$f_{\boldsymbol{y}|\boldsymbol{s},H}(\boldsymbol{y}|\boldsymbol{s} = \tilde{\boldsymbol{s}}, H). \tag{3.5}$$

Eq. (3.4) is referred to as the ML criterion and the detector given by

$$\tilde{\boldsymbol{s}}_{\mathrm{ML}} = \underset{\tilde{\boldsymbol{s}} \in S}{\operatorname{argmax}} \; f_{\boldsymbol{y}|\boldsymbol{s},H}(\boldsymbol{y}|\boldsymbol{s} = \tilde{\boldsymbol{s}}, H) \tag{3.6}$$

is referred to as the ML detector. Note that the ML detector is always given by Eq. (3.5) even in the case where $\mathrm{P}(\mathrm{s} = \tilde{\mathrm{s}})$ is not constant, i.e. when symbols are transmitted with nonuniform probabilities, but that in this case it is not optimal in the sense that it maximizes the probability of obtaining the transmitted message. Eq. (3.5) may be further simplified by applying the model of Eq. (3.1) to obtain

$$f_{\boldsymbol{y}|\boldsymbol{s},H}(\boldsymbol{y}|\boldsymbol{s}=\tilde{\boldsymbol{s}},H)=f_{\boldsymbol{n}}(\boldsymbol{y}-H\tilde{\boldsymbol{s}}). \tag{3.7}$$

Further, note that the probability density of the white Gaussian noise $\boldsymbol{n}$ is given by

$$f_{\boldsymbol{n}}(\boldsymbol{n})=\frac{1}{(\pi\sigma^2)^n}e^{-\frac{1}{\sigma^2}\|\boldsymbol{n}\|^2}. \tag{3.8}$$

Thus, the likelihood of $\tilde{\mathbf{s}}$ is obtained by substituting $\mathbf{n}$ with $\mathrm{n}\triangleq\ \boldsymbol{y}-H\tilde{\boldsymbol{s}}$ in the above. By observing that $\mathrm{f}_{\mathrm{y|s,H}}$ is maximized by minimizing $\|\boldsymbol{n}\|^2$ the ML estimate of $\boldsymbol{s}$, i.e. $\tilde{\mathrm{s}}_{\mathrm{ML}}$, is given by

$$\tilde{\boldsymbol{s}}_{\mathrm{ML}}=\underset{\tilde{\boldsymbol{s}}\in S}{\operatorname{argmax}}\ \|\boldsymbol{y}-H\tilde{\boldsymbol{s}}\|^2. \tag{3.9}$$

Thus, the ML detector chooses the message $\tilde{\boldsymbol{s}}$ which yields the smallest distance between the received vector $\boldsymbol{y}$ and hypothesized message $H\tilde{s}$. Although the ML detector has the best performance compared to other detectors, its computational complexity exponentially grows with the size of the problem due to the exhaustive search used in the algorithm.

3.2.2. Zero-forcing detection

Zero-Forcing (ZF) detection refers to a form of linear equalization algorithm used in communication systems which applies the inverse of the frequency response of the channel [23]. The ZF technique nullifies the interference by the following weight matrix

$$\mathrm{W}_{\mathrm{ZF}}=(H^{\mathrm{H}}H)^{-1}H^{\mathrm{H}}. \tag{3.10}$$

where $(.)^{\mathrm{H}}$ denotes the Hermitian transpose operation. Therefore, it inverts the effect of channel as

$$\tilde{\boldsymbol{s}}_{\mathrm{ZF}}=\mathrm{W}_{\mathrm{ZF}}\boldsymbol{y}=\boldsymbol{s}+(H^{\mathrm{H}}H)^{-1}H^{\mathrm{H}}\boldsymbol{n}=\boldsymbol{s}+\tilde{\boldsymbol{n}}_{\mathrm{ZF}}. \tag{3.11}$$

where $\tilde{\boldsymbol{n}}_{\mathrm{ZF}}=(H^{\mathrm{H}}H)^{-1}H^{\mathrm{H}}\boldsymbol{n}$ is the so called processed noise. ZF detection algorithm is a linear detection algorithm since it behaves as a linear filter separating different data streams to perform decoding independently on each stream, therefore eliminating the multi-stream interference. The drawback of ZF detection is retarded BER performance due to noise enhancement. The additive white Gaussian noise (AWGN) loses its whiteness property it is enhanced and correlated across the data streams.

3.2.3. Minimum mean square error detector

In order to maximize the post-detection SINR, the MMSE weight matrix is given as

$$\mathrm{W}_{\mathrm{MMSE}}=(H^{H}H+N_0I)^{-1}H^{H}. \tag{3.12}$$

Therefore, the estimate of the transmission symbol $\boldsymbol{s}$ can be obtained as:

$$\begin{aligned}\tilde{\boldsymbol{s}}_{\mathrm{MMSE}}&=\mathrm{W}_{\mathrm{MMSE}}\boldsymbol{y}=(H^{H}H+N_0I)^{-1}H^{H}\boldsymbol{y}\\&=\boldsymbol{s}+(H^{H}H+N_0I)^{-1}H^{H}\boldsymbol{n}=\boldsymbol{s}+\tilde{\boldsymbol{n}}_{\mathrm{MMSE}},\end{aligned} \tag{3.13}$$

where $\tilde{\boldsymbol{n}}_{\mathrm{MMSE}} = (H^H H + N_0 I)^{-1} H^H \boldsymbol{n}$ is the processed noise. And MMSE receiver requires the statistical information of noise N_0. MMSE detectors balance the noise enhancement and multi-stream interference by minimizing the total error [24].

3.2 OFDMA in Full-duplex communications with three detection methods

In this simulation, we assume the joint cancellation has been implied, but residual self-interference still affects the system performance. Therefore, BER performance analysis of the OFDMA based system is analyzed. No interference between users is assumed and the above mentioned detection schemes have been used for the analysis. Simulation parameters are listed in the Table 3.1. The desired signal channel is a multipath channel simulated according to the [35].

Table 3.1. Full-duplex OFDMA system simulation parameters.

Parameter	Value
bandwidth, b	20 MHz
number of subcarriers, N_{sub}	2048
local node transmit power, P_t^{ln}	20 dBm
remote node transmit power, P_t^{rn}	0 ~ 20 dBm
desired signal channel path-loss, $L_{\mathrm{p}}^{\mathrm{D}}$	70 dB
receiver noise level, N_{r}	-100 dBm
transmitter noise level, N_{t}	$P_t^{\mathrm{ln}} - 30$ dBm
Residual SI Channel	Rayleigh and Rice fading
Modulation	QPSK
Number of user	5

Fig. 3.3 demonstrates the BER performance of an OFDMA full-duplex system for different values of residual self-interference powers. The residual self-interference is assumed a random variable with Rayleigh distribution. It is observed that as the residual self-interference power is reduces the BER drops as expected.

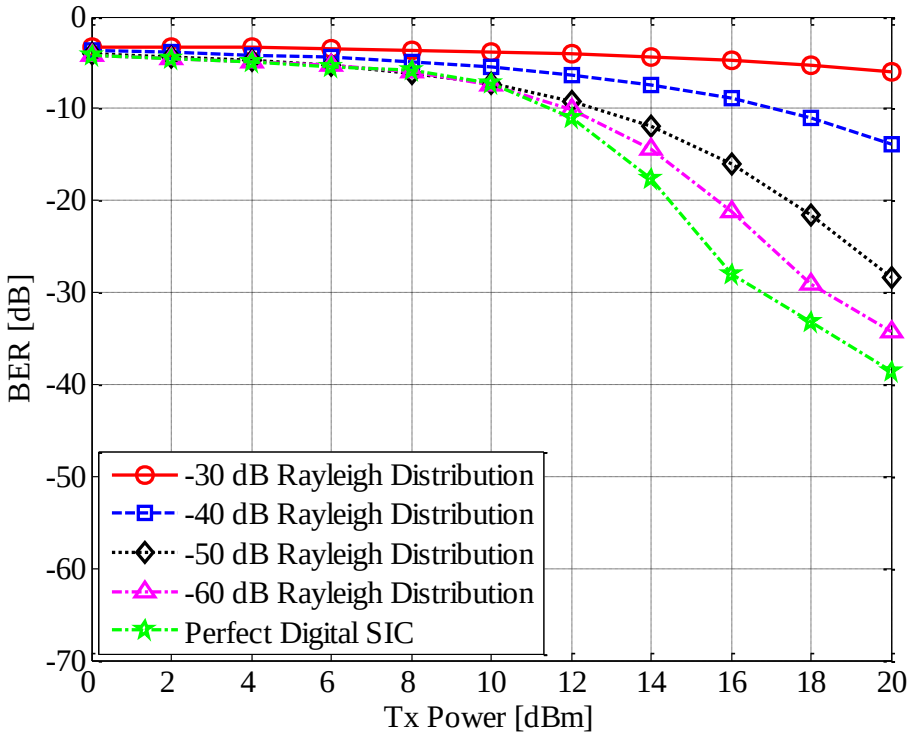

Fig. 3.3 full-duplex OFDMA BER performance for different residual self-interference where residual self-interference is assumed random variable with Rayleigh distribution.

Fig. 3.4 shows the full-duplex OFDMA BER performance for different values of residual self-interference powers, where residual self-interference assumed random value with Rician distribution. It is clearly shown that the BER performance is good with the lower RSI power.

In addition, BER performance for different detection schemes in a full-duplex OFMDA system are compared in Fig. 3.5, where the Rayleigh and Rician distributions are assumed for the residual self-interference with a power of -50 dB. It is observed that the BER performance of the system when the residual self-interference has a Rician distribution is better compared to that of Rayleigh distribution. In Fig. 3.5, the BER performance of ZF, MMSE and ML are almost the same, because in this section we only consider the point-to-point system so that inter-symbol interference does not exist. However, the complexity of the detections are different, i.e. for the ZF is the length of FFT (L) * the number of symbols in a block (N), namely, NL; for the MMSE is (L+2) N and for ML is $2^Q NL$, Q is number of bits.

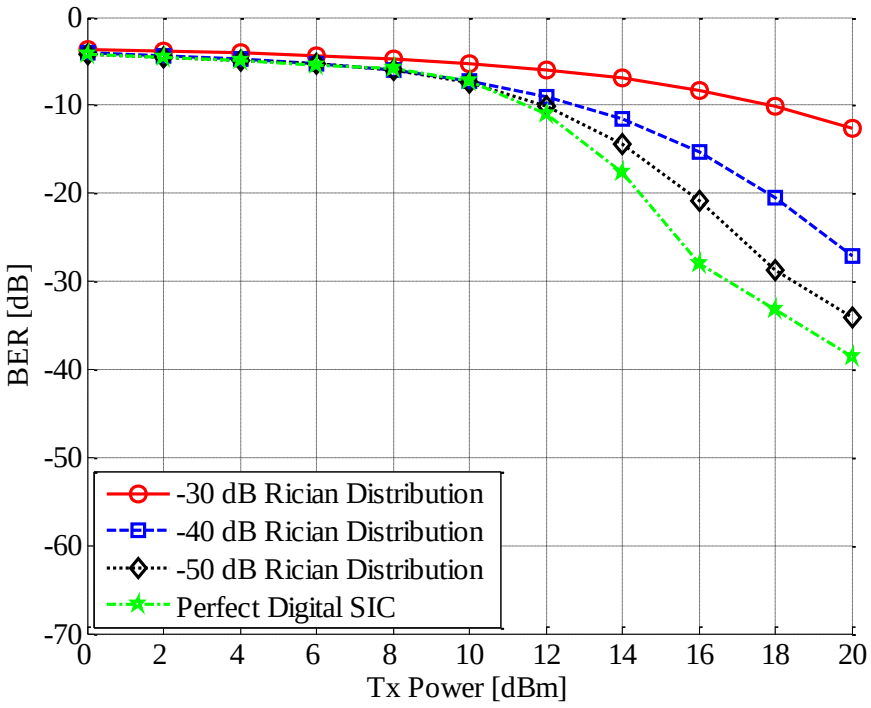

Fig. 3.4 full-duplex OFDMA BER performance for different residual self-interference where residual self-interference is random variable with Rice distribution.

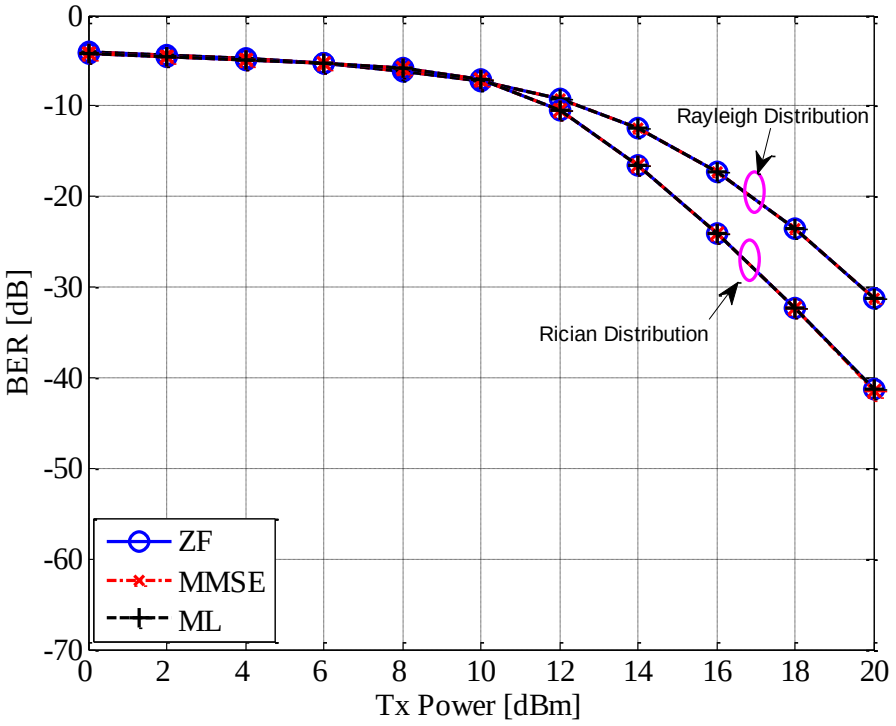

Fig. 3.5 The comparison BER performance between the different detection schemes with the Rayleigh and Rician distributed residual self-interference in OFMDA system.

3.3. SC-FDMA for full-duplex systems

In this section, we assume the joint cancellation has been implied, but residual self-interference still exists. BER analysis of an SC-FDMA based system is derived similar to those for OFDMA and using the previously discussed detection schemes. Simulation parameters are found in Table 3.2. The desired signal channel is a multipath channel simulated according to the [35].

Table 3.2. Full-duplex SC-FDMA system Simulation parameters.

Parameter	Value
bandwidth, b	20 MHz
number of subcarriers, N_{sub}	2048
local node transmit power, P_t^{ln}	20 dBm
remote node transmit power, P_t^{rn}	0 ~ 20 dBm
desired signal channel path-loss, L_{p}^{D}	70 dB
receiver noise level, N_{r}	-100 dBm
transmitter noise level, N_{t}	$P_t^{\text{ln}} - 30$ dBm
Residual SI Channel	Rayleigh and Rice fading
Modulation	QPSK
DFT & IDFT size	2048

The full-duplex SC-FDMA BER performance is presented in Fig. 3.6 for different residual self-interference powers. Residual self-interference power is assumed a Rayleigh distributed random variable. As expected with lower residual self-interference power, the BER is decreased.

Fig. 3.7 shows the full-duplex SC-FDMA system BER performance for various values of residual self-interference powers, where residual self-interference power is assumed a random variable with a Rician distribution. Again for lower residual self-interference power the BER performance improves as it is expected.

Finally, Fig. 3.8 demonstrates the BER performance of three detection schemes in the full-duplex SC-FDMA system. Here the residual self-interference power distribution is assumed Rayleigh and Rician and the residual self-interference power is -40 dB. The BER performance of the Rician case is better than that of Rayleigh case. The complexities of three detection schemes are the same as the OFDMA case.

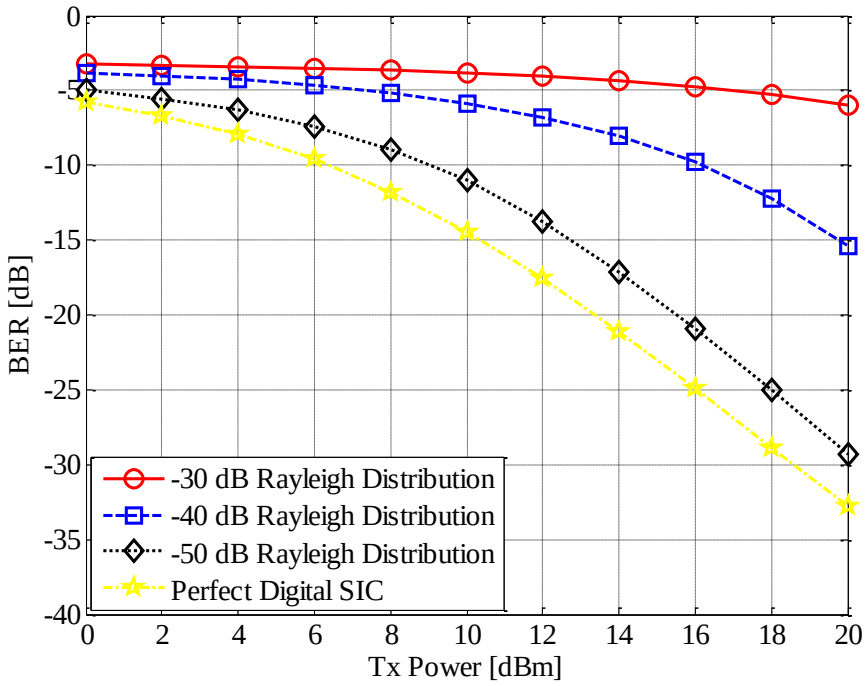

Fig. 3.6 full-duplex SC-FDMA system BER performance for different residual self-interference (Rayleigh Distribution) powers.

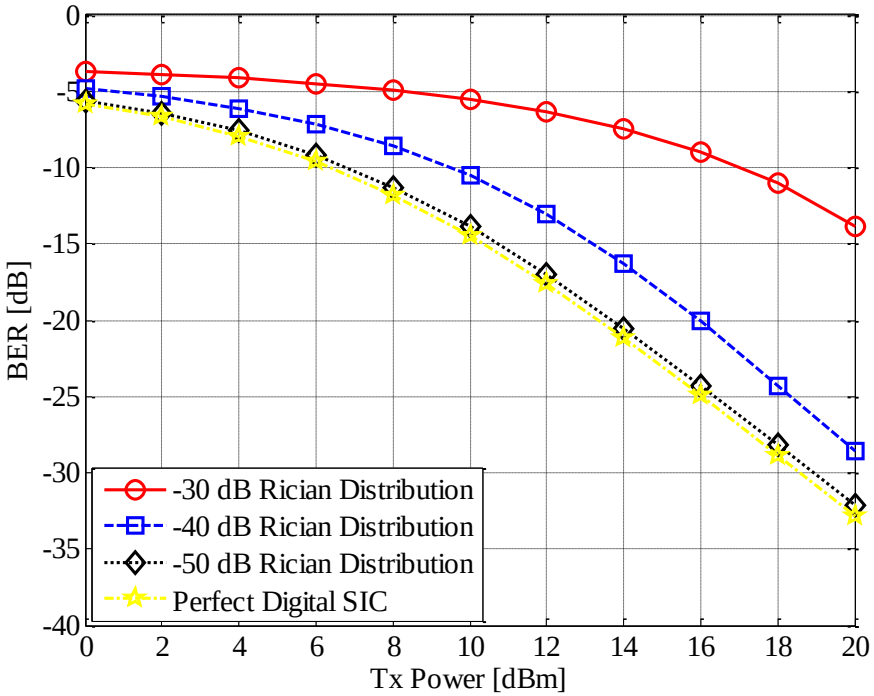

Fig. 3.7 full-duplex SC-FDMA system BER performance for different residual self-interference (Rician Distribution) powers.

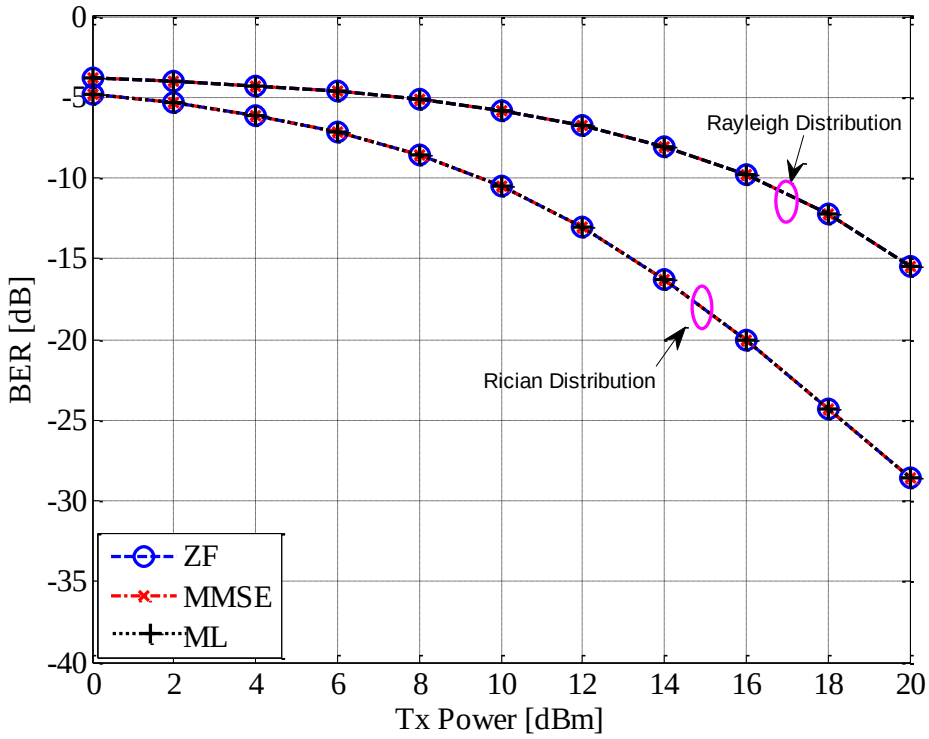

Fig. 3.8 The comparison BER performance between the different detection schemes with the Rayleigh and Rician distributed residual self-interference in SC-FDMA system.

3.4. Summary

In this section, although it is assumed that self-interference cancellation and isolation at antenna, RF and digital baseband is employed, but there a residual self-interference is remained. Therefore, the performance of multiple access schemes (OFDMA and SC-FBMA) for a full-duplex system with three detection schemes is investigated when residual self-interference exist after joint cancellation. According to the simulation results, the BER performance of ZF, MMSE and ML are almost the same, because we only consider the point-to-point system so that inter symbol interference does not exist. The only difference is the complexity of calculation which for the ZF is the length of FFT (L) * the number of symbols in a block (N), namely, NL; for the MMSE is (L+2) N and for ML $2^Q NL$, Q is number of bits. In the future, we will focus on the system performance for the full-duplex MIMO system with the different liner/non-liner detection schemes.

4. Digital self-interference cancellation for full-duplex MIMO systems

4.1. Motivation

As it was discussed in the introduction, the self-interference, which is the main difficulty for full-duplex transmission, is a more complex issue in full-duplex MIMO system operation. Since this deliverable deals with the solutions in digital baseband, here we assume that the self-interference cancellation at RF is achieved which together with a reasonable transmit-receive isolation can cancel out significant amount of the self-interference, but it is reasonable to assume that a remaining residual self-interference exists in the digital baseband domain. This motivates us to develop robust signal processing techniques to mitigate the residual self-interference in the digital baseband of the full-duplex MIMO system. In this section we first discuss the straight forward self-interference cancellation for full-duplex MIMO. The performance of this cancellation is based on the self-interference channel estimate. In case there is an error in the channel estimation, or there are nonlinear components which are not cancelled, a residual self-interference is remained. To cancel the self-interference further, low complexity precoding methods are introduced, analysed and simulated. The influence of self-interference channel estimation error is analyzed on the performance of the system as well.

4.2. System model

The block diagram for the assumed full-duplex MIMO system with two identical transceivers is shown in Fig. 4.1. Each transceiver equipped with M transmit antennas and N receive antennas. Perfect synchronization is also assumed. As depicted in Fig. 4.1, the desired channel between the transmitter node $j \in (1,2)$ and the receiver node $i \in (1,2)$ is denoted as $H_{ji} \in \mathrm{C}^{\mathrm{N_i} \times \mathrm{M_j}}$, while the MIMO self-interference channel from the transmitter node $i \in (1,2)$ to itself is denoted as $H_{ii} \in \mathrm{C}^{\mathrm{N_i} \times \mathrm{M_i}}$. Note that elements of the MIMO self-interference channel matrix are assumed random variables with Rayleigh distribution. This makes sense assuming multipath in the self-interference channel and considering that main components is cancelled in the self-interference cancellation process. The received signal at the receiver node i is expressed as:

$$\mathbf{y}_i = \sqrt{\rho_i}\mathbf{H}_{ji}\mathbf{x}_j + \sqrt{\eta_i}\mathbf{H}_{ii}\mathbf{x}_i + \mathbf{n}_i \,, \tag{4.1}$$

where $\rho_i > 0$ indicates the average gain of the desired channel while $\eta_i > 0$ denotes the average gain in the residual self-interference channel at node i after RF cancellation and achieved isolation in the full duplex transmit-receive path. $\mathbf{n}_i \in \mathbf{C}^{N_i \times 1}$ represents the complex AWGN with zero mean and covariance matrix $\sigma_n^2 I_N$.

The design of transmission strategies for a full-duplex MIMO system is even more challenging because of the self-interference in the system. Clearly, the desired transmit technique must provide a trade-off between system performance and algorithm complexity.

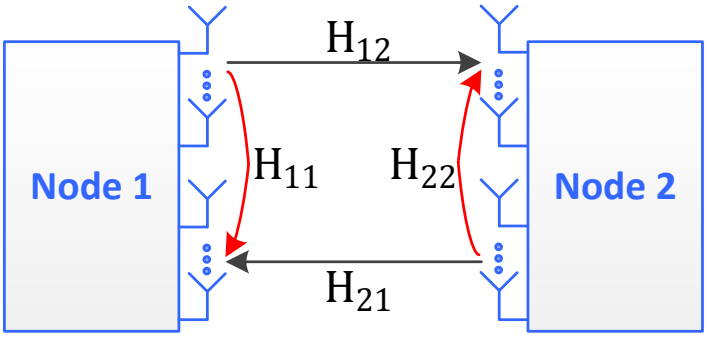

Figure 4.1. Block diagram of a full-duplex MIMO system.

4.2. Digital self-interference cancellation for full-duplex MIMO system

In the full-duplex MIMO system, since each receiver node i knows its own transmitted signal $\mathbf{x}_i$ the self-interference cancellation using an estimate of the MIMO self-interference channel is straight forward. The residual self-interference could be simply subtracted from the received signal using $\mathbf{x}_i$. Considering the error in the self-interference channel estimate it can be expressed as

$$\hat{\mathbf{H}}_{ii} = \mathbf{H}_{ii} + \mathbf{H}_e , \tag{4.2}$$

where the channel estimation errors is represented by a matrix of dimension $N_i \times M_i$, its elements are assumed to be i.i.d. zero-mean complex Gaussian with variance σ_e^2. Furthermore, the random quantities $\mathbf{H}_{ii}$, $\mathbf{x}_i$ and $\mathbf{H}_e$ are assumed independent. Thus the Eq. (4.1) could be rewritten again as

$$\mathbf{y}_i = \sqrt{\rho_i}\mathbf{H}_{ji}\mathbf{x}_j + \sqrt{\eta_i}\left(\mathbf{H}_{ii} - \hat{\mathbf{H}}_{ii}\right)\mathbf{x}_i + \mathbf{n}_i . \tag{4.3}$$

On the other hand if a perfect self-interference channel estimate is available, the self-interference can be perfectly removed, so that the received signal can be expressed similarly to a half-duplex system as

$$\mathbf{y}_i = \sqrt{\rho_i}\mathbf{H}_{ji}\mathbf{x}_j + \mathbf{n}_i . \tag{4.4}$$

4.3. Precoding for full-duplex MIMO systems

The aim of any precoding introduced for full-duplex MIMO system is to reduce/cancel any remaining residual self-interference. Assuming the data symbol vector is denoted as $\mathbf{s}_i \in \mathbf{C}^{L\times 1}$ at node i, where L is the number of parallel transmitted data symbols which is precoded using the precoding matrix $\mathbf{T}_i \in \mathbf{C}^{M_i \times L}$, the transmitted symbol vector is given by

$$\mathbf{x}_i = \mathbf{T}_i\mathbf{s}_i . \tag{4.5}$$

Then, the received signal in Eq. (4.1) can be rewritten as:

$$\mathbf{y}_i = \sqrt{\rho_i}\mathbf{H}_{ji}\mathbf{T}_j\mathbf{s}_j + \sqrt{\eta_i}\mathbf{H}_{ii}\mathbf{T}_i\mathbf{s}_i + \mathbf{n}_i . \quad (4.6)$$

Here, first the Zero-Forcing (ZF) precoder is introduced for this purpose and then SLNR based precoder is analyzed as a further improvement [25].

4.3.1. ZF precoding

Our primary objective is to select a nonzero matrix $\mathbf{T}_i$ for node i at the receiver where the residual self-interference is eliminated completely ($\mathbf{H}_{ii}\mathbf{T}_i$ = 0), as shown in Fig. 4.2. The ZF precoding scheme can cancel the residual self-interference perfectly. Note that the precoding matrix $\mathbf{T}_i$ should be a nonzero matrix, otherwise no signal is transmitted. To guarantee the existence of a nonzero precoding matrix, a sufficient condition is that the number of the transmit antennas M_i is larger than the sum of the number of receiver antennas N_j and the self-interference receiver antennas N_i that is

$$M_i \geq N_i + N_j . \quad (4.7)$$

In this scenario, the received signal at node i could be expressed as:

$$\mathbf{y}_i = \sqrt{\rho_i}\mathbf{H}_{ji}\mathbf{T}_j\mathbf{s}_j + \mathbf{n}_i . \quad (4.8)$$

Under this sufficient condition, let us denote $\mathbf{V}_{ii} \in \mathbf{C}^{M_i \times n_u}$, $n_u > M_i - N_i$, is the null-space of $\mathbf{H}_{ii}$, which can be derived by SVD as [26]:

$$\mathbf{H}_{ii} = \left[\tilde{\mathbf{U}}_{ii}\ \mathbf{U}_{ii}\right] \cdot \begin{bmatrix} \sum & \mathbf{0} \\ \mathbf{0} & \mathbf{0} \end{bmatrix} \cdot \begin{bmatrix} \tilde{\mathbf{V}}_{ii}^H \\ \mathbf{V}_{ii}^H \end{bmatrix}, \quad (4.9)$$

where columns of $\mathbf{V}_{ii}$ and $\tilde{\mathbf{V}}_{ii}$ form an orthonormal basis for the channel, with $\tilde{\mathbf{V}}_{ii} \in \mathbf{C}^{M_i \times n_s}$ being the signal space of the channel and rich-scattering is assumed with $M_i > N_i$. The precoding matrix then may be chosen as

$$\mathbf{T}_i = \mathbf{V}_{ii}\mathbf{A}_{ii} , \quad (4.10)$$

where $\boldsymbol{A}_{ii}$ is a nonzero $n_u \times L$ ZF precoding matrix. As expected, the ZF scheme can completely cancel the residual self-interference at the receiver node i. However, this solution is sensitive to other interferences and other sources of distortion, such as channel estimation errors.

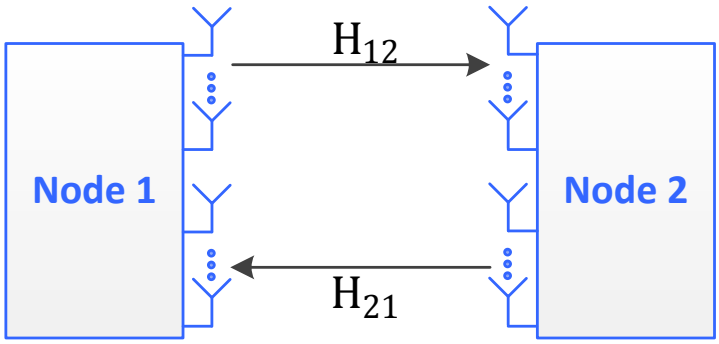

Figure 4.2. Block diagram of the full-duplex MIMO system with perfect self-interference cancellation, which works like a half-duplex system.

4.3.2. SLNR-based precoding

It is well known that although ZF precoding cancels the residual self-interference well, but it can enhance the system noise and leave a small SNR. The ZF precoding also imposes a condition on the relation between the numbers of transmit and receive antennas. An alternative scheme that relaxes the requirement Eq. (4.7) and takes the noise contribution into account when choosing $\mathbf{T}_i$, is the SLNR-based precoding.

The SLNR-based precoding avoids the joint design of the precoders between two transceiver devices and can lead to a closed form characterization of the optimal $\mathbf{T}_i$ in terms of generalized eigenvalue problems. Moreover, the SLNR-based precoding does not require the limitation on the number of transmit and receive antenna $n_u > M_i - N_i$. It is observed from Eq. (4.6) that the power of the desired signal for node i is given by $\left\|\sqrt{\rho_i}\mathbf{H}_{ji}\mathbf{T}_j\right\|^2$ and the power of the self-interference that is caused by node i is given by $\left\|\sqrt{\eta_i}\mathbf{H}_{ii}\mathbf{T}_j\right\|^2$ and $\|.\|$ denotes Euclidian norm. We would also like $\left\|\sqrt{\rho_i}\mathbf{H}_{ji}\mathbf{T}_j\right\|^2$ to be large compare to the power leakage from node i to its own receiver part for the efficiency purposes. These considerations motivate us to introduce a figure of merit in terms of SLNR defined as

$$\mathrm{SLNR_i} = \frac{\left\|\sqrt{\rho_i}\mathbf{H}_{ij}\mathbf{T}_i\right\|^2}{N_i\sigma_n^2 + \left\|\sqrt{\eta_i}\mathbf{H}_{ii}\mathbf{T}_i\right\|^2} \tag{4.11}$$

Thus note that in interference limited scenarios, the criterion reduces to maximizing the ratio $\left\|\sqrt{\rho_i}\mathbf{H}_{ij}\mathbf{T}_i\right\|^2 / \left\|\sqrt{\eta_i}\mathbf{H}_{ii}\mathbf{T}_i\right\|^2$. Maximizing this quantity for desired signal in the system simultaneously will improve the SIR. On the other hand, in noise limited scenarios, the

optimization criterion reduces to maximizing the SNR, $\left\|\sqrt{\rho_i}\mathbf{H}_{ij}\mathbf{T}_i\right\|^2/N_i\sigma_n^2$. Using this concept of leakage, Eq. (4.11), the following decoupled optimization problem can be formulated as [27]

$$\mathbf{T}_i^o = \underset{\mathbf{T}_i \in C^{N_i \times 1}}{\operatorname{argmax}} \frac{\left\|\sqrt{\rho_i}\mathbf{H}_{ij}\mathbf{T}_i\right\|^2}{N_i\sigma_n^2+\left\|\sqrt{\eta_i}\mathbf{H}_{ii}\mathbf{T}_i\right\|^2}. \tag{4.12}$$

To solve Eq. (4.12) we note that, in view of the Rayleigh-Ritz quotient result [28], the optimum beamforming $\mathbf{T}_i^o$ vector is given by

$$\mathbf{T}_i^o \propto \text{max. generalized eigenvector } (\mathbf{H}_{ij}^H\mathbf{H}_{ij},\ N_i\sigma_i^2\mathbf{I}+\mathbf{H}_{ii}^H\mathbf{H}_{ii}) \tag{4.13}$$

in terms of the eigenvector corresponding to the largest generalized eigenvalue of the matrices $\mathbf{H}_{ij}^H\mathbf{H}_{ij}$ and $N_i\sigma_i^2\mathbf{I}+\mathbf{H}_{ii}^H\mathbf{H}_{ii}$. Since $N_i\sigma_i^2\mathbf{I}+\mathbf{H}_{ii}^H\mathbf{H}_{ii}$ is invertible, the generalized eigenvalue problem Eq. (4.13) actually reduces to a standard eigenvalue problem, namely

$$\mathbf{T}_i^o \propto \text{max. eigenvector}\left(\left(N_i\sigma_i^2\mathbf{I}+\mathbf{H}_{ii}^H\mathbf{H}_{ii}\right)^{-1}\mathbf{H}_{ij}^H\mathbf{H}_{ij}\right), \tag{4.14}$$

The proportionality constant is chosen such that the norm of $\mathbf{T}_i^o$ is scaled to $\|\mathbf{T}_i^o\|^2 = 1$.

4.4. Precoding with digital self-interference cancellation

It is observed that the precoding techniques discussed in the previous section do not use any knowledge of the transmitted signal. On the other hand, since the transmitted signal is known, the self-interference can be cancelled at the digital baseband using an estimate of the self-interference channel. In this case, the precoding techniques can improve the performance by removing the residual self-interference as much as possible. The system equation in this case can be expresses as

$$\mathbf{y}_i = \sqrt{\rho_i}\mathbf{H}_{ji}\mathbf{T}_j\mathbf{s}_\mathbf{j} + \sqrt{\eta_i}\left(\mathbf{H}_{ii} - \hat{\mathbf{H}}_{ii}\right)\mathbf{T}_i\mathbf{s}_i + \mathbf{n}_i\,. \tag{4.15}$$

Following equations (4.8) - (4.11), the optimum $\mathbf{T}_i^o$ vector is given by

$$\mathbf{T}_i^o \propto \text{max. eigenvector}\left((N_i\sigma_i^2\mathbf{I}+\mathbf{H}_e^H\mathbf{H}_e)^{-1}\mathbf{H}_{ij}^H\mathbf{H}_{ij}\right). \tag{4.16}$$

4.5. Simulation results and discussion

The discussed the self-interference cancellation using the self-interference channel estimate, precoding approaches with no prior digital self-interference cancellation, and precoding after

digital self-interference cancellation are simulated and the performances are investigated. The simulation parameters can be found in Table 4.1. For the comparison purpose, both BER results and sum-rate curves are presented for different number of MIMO channels.

Figure 4.3 demonstrates the SNR performance of the precoding-based cancellation schemes with Rayleigh fading channels with different residual self-interference values and with perfect CSI knowledge. Note that two cases are used as benchmark, namely half-duplex and no digital self-interference cancellation. In this figure, blue curves show the performance of the SLNR-based schemes, red curves represent the ZF performance, and the black curves are the benchmark schemes. In this case the condition of Eq. (4.7) is satisfied, i.e. $M_i = 4, N_i = 2, N_j = 2$. When the residual self-interference is low, i.e. $\sqrt{\eta_i}$= 0 dB, the SLNR-based scheme outperforms the ZF by approximately 2 dB at a BER of 10^{-4}. When the residual self-interference increases to 20 dB, the ZF outperforms the SLNR-based scheme by approximately 6 dB at a BER of 10^{-4}. This is due to the fact that the ZF scheme can mitigate the residual self-interference completely, no matter how large it is. However, as expected, when the condition of Eq. (4.7) is not satisfied, i.e. $M_i = 3$, $N_i = 3, N_j = 3$, the BER performance versus SNR for the ZF scheme is much worse than the SLNR scheme.

Figure 4.4 presents the BER performance versus SNR of both the precoding schemes and the digital self-interference cancellation for full-duplex MIMO systems, with different channel estimation errors, at SNR = 10 dB in the case of the residual self-interference channel gain $\sqrt{\eta_i}$ = 20 dB. It is observed that when the channel estimation errors are lower than -17 dB, the digital self-interference cancellation alone outperforms both precoding techniques, but with the increase of the self-interference channel estimation errors, the precoding schemes present a better performance.

Finally, by using both digital self-interference cancellation and then precoding, Fig. 4.5 shows the BER performance versus SNR with perfect CSI and $\sqrt{\eta_i}$ = 20 dB. It is observed that, with the joint SLNR-bases precoding and digital self-interference cancellation, there is 8 dB improvement at a BER of 10^{-3} compared to precoding alone. This outperforms the joint ZF precoding and digital self-interference cancellation by around 2 dB at BER = 10^{-3}. As mentioned previously, ZF imposes limitation on the number of MIMO channels through Eq. (4.7). Since this is not a requirement for the SLNR-bases precoding approach, Fig. 4.6 presents the joint SLNR-based precoding and the digital self-interference for $\sqrt{\eta_i}$ = 1 dB, $M_i = 3, N_i = 3, N_j = 3$. In this case, the BER is improved by approximately 14 dB at a BER=10^{-3}, compared to the SLNR-based precoding alone. The sum-rate of the full-duplex MIMO system is also characterized, and it shows the same trend as the BER performance. Fig. 4.7 shows the sum-rate of both the full-duplex and half-duplex systems. It is notable that the half-duplex link is used ad benchmark to for the joint SLNR-predcoding and digital self-interference cancellation. The gain achieved by this approach pushes the full-duplex system performance toward doubling the half-duplex performance.

Table 4.1. Simulation Parameters

Parameter	Half-Duplex	Full-Duplex
Transmit Antennas at each node	3	4, 3
Receive Antennas at each node	3	2, 3
Modulation	QPSK	
Precoding Schemes	ZF, SLNR-based	
Residual Self-Interference Channel	-	Uncorrelated Rayleigh fading channel
Desired Signal Channel	Uncorrelated Rayleigh fading channel	
Channel realizations	50,000	

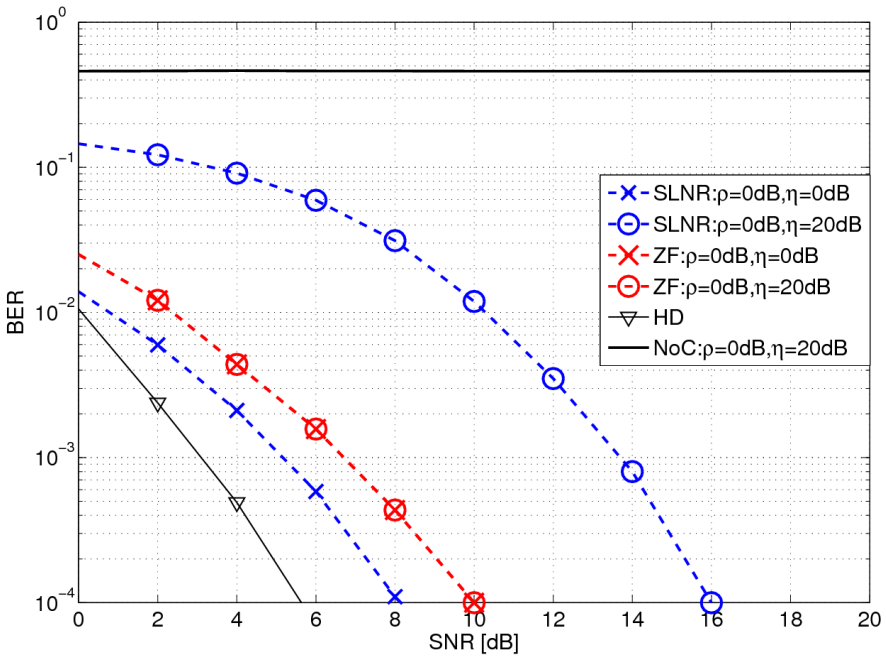

Figure 4.3. The BER performance of ZF and SLNR-based precoding schemes, $M_i = 4, N_i = 2, N_j = 2$.

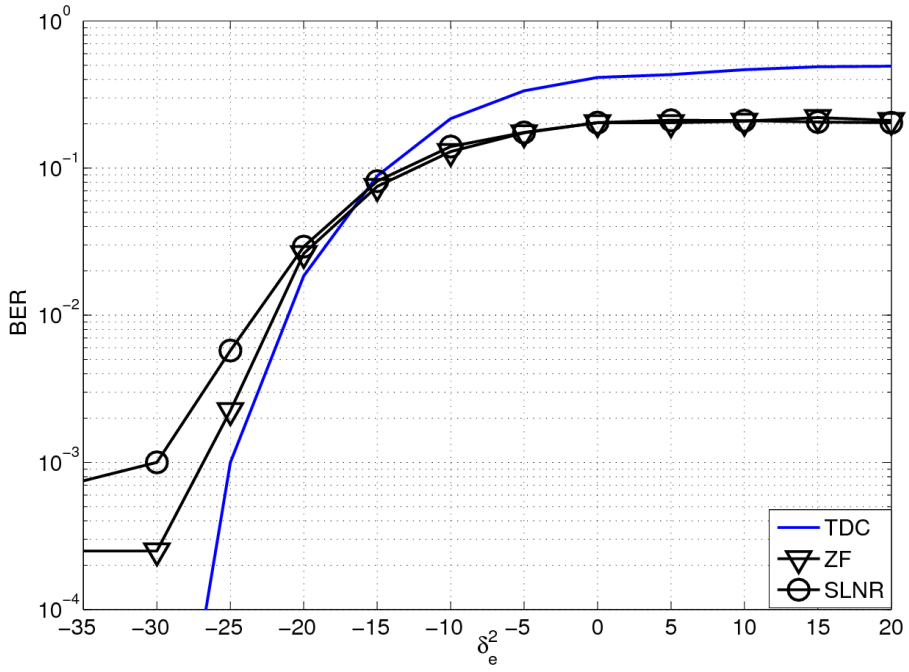

Figure 4.4. Impact of the self-interference channel estimation error on the BER performance of the full-duplex MIMO system using digital self-interference cancellation, ZF or SLNR-based precoding, where $M_i = 4$, $N_i = 2$, $N_j = 2$, $\sqrt{\eta_i}$ = 20 dB, SNR = 10 dB.

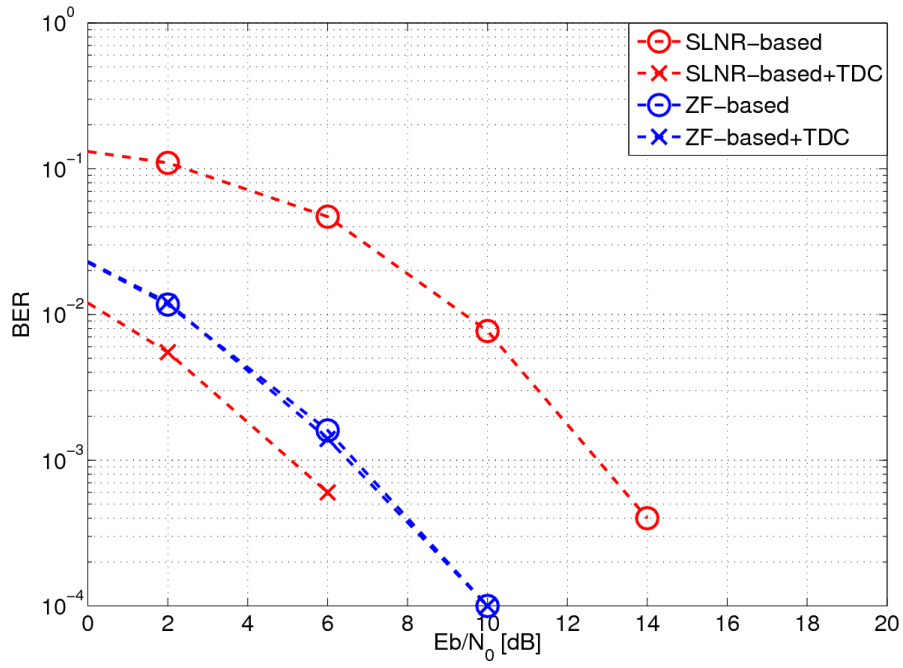

Figure 4.5. The BER performance for both precoding schemes, with and without digital self-interference cancellation, $M_i = 4$, $N_i = 2$, $N_j = 2$, (TDC indicates digital self-interference cancellation).

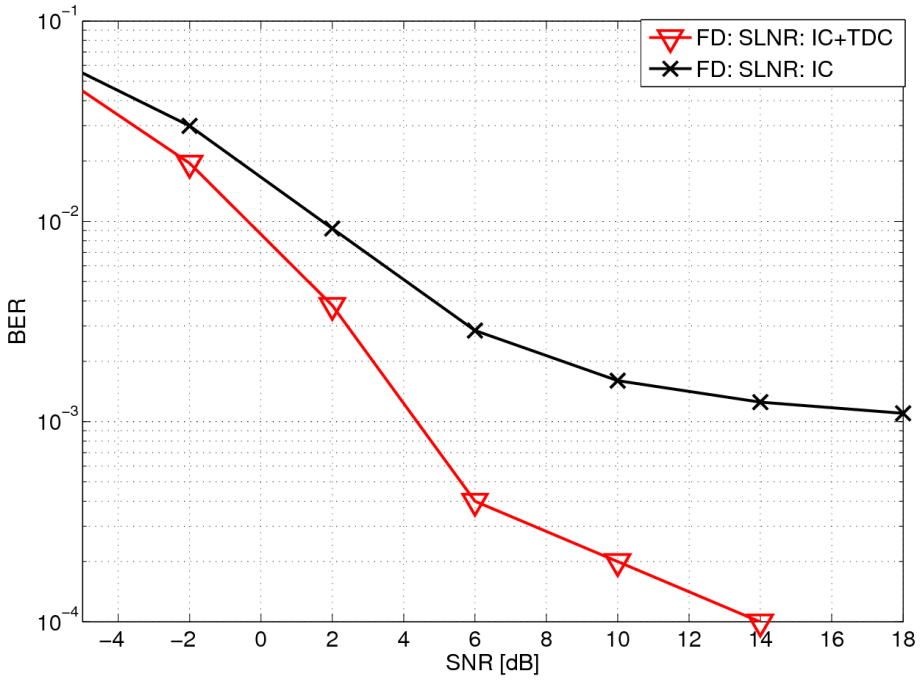

Figure 4.6. The BER performance, for SLNR-based precoding with and without digital self-interference cancellation, $M_i = 3$, $N_i = 3$, $N_j = 3$, (IC indicates imperfect channel estimation).

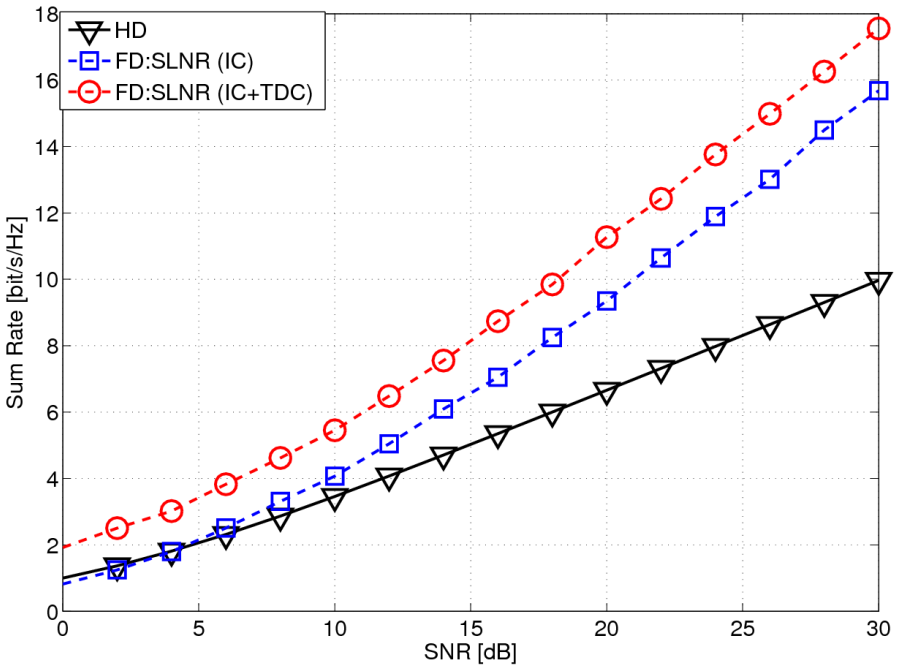

Figure 4.7. The sum-rate for half-duplex system, and SLNR-based precoding, with and without the digital self-interference cancellation, $M_i = 3$, $N_i = 3$, $N_j = 3$.

4.6. Performance of full-duplex MIMO in point-to-point and relay links

4.6.1. Full-duplex MIMO point-to-point link

A full-duplex point-to-point network is shown in Fig. 4.1, where there are nodes 1 and 2 can be local or remote nodes. Each node has N_s and N_r transmission and receiving antenna, respectively. The desired signal MIMO channels from node 1 to node 2, from node 2 to node 1, are indicated as $\mathbf{H}_{12}$, $\mathbf{H}_{21}$, and the self-interference channel at node 1 and node 2 are indicated as $\mathbf{H}_{11}$ and $\mathbf{H}_{22}$, respectively. Let ρ_i and η_i are the average signal transmission power for node i, $i \in (1,2)$, respectively. All noises are assumed AWGN and the $\mathbf{H}_{12}$ and $\mathbf{H}_{21}$ channels are assumed to 802.11 multipath channels with the channel state information available at both link ends.

For the half-duplex system, the received signal at the i th receiver is expressed in Eq. (4.4). The avarage SNR at the i th receiver can be obtained as

$$\gamma_i^{\mathrm{HD}} = \frac{\rho_i}{\sigma_i^2}\,. \tag{4.17}$$

Therefore, the average rate of half-duplex is obtained by [29]:

$$R_i^{\mathrm{HD}} = \mathrm{E}_{\mathbf{H}_{ij}}\left[\log_2 \det\left(\mathbf{I} + \frac{\gamma_i^{\mathrm{HD}}}{N_s}\mathbf{H}_{\boldsymbol{ij}}^{H}\mathbf{H}_{ij}\right)\right]. \tag{4.18}$$

where $\mathrm{E}[.]$ denotes expectation. On the other hand, for the full-duplex link, According to Eq. (4.1), the average SINR at the i th receiver can be obtained as

$$\gamma_i^{\mathrm{FD}} = \frac{\rho_i}{\eta_i+\sigma_n^2}. \tag{4.19}$$

Therefore, the the average rate of full-duplex is obtained by

$$R_i^{\mathrm{FD}} = \mathrm{E}_{\mathbf{H}_{ij}}\left[\log_2 \det\left(\mathbf{I} + \frac{\gamma_i^{\mathrm{FD}}}{N_s}\mathbf{H}_{\boldsymbol{ij}}^{H}\mathbf{H}_{ij}\right)\right]. \tag{4.20}$$

Figure 4.8 compares capacity of the point-to-point link half-duplex and half-duplex with perfect self-interference cancellation. It is clearly shown that the capacity of full-duplex scheme is twice than that of half-duplex with perfect self-interference cancellation. When the self-interference is not fully cancelled, Fig. 4.9 shows the capacity of the full-duplex point-to-point link compared to those of the half-duplex. It is observed that with the more residual self-interference remained in the system full-duplex link capacity is decreased. When residual self-interference is large, the capacity of full-duplex is less than that of half-duplex, i.e., when the SNR is less 18 dB, the capacity of full-duplex, with residual self-interference of 10 dB, is less than that of half-duplex.

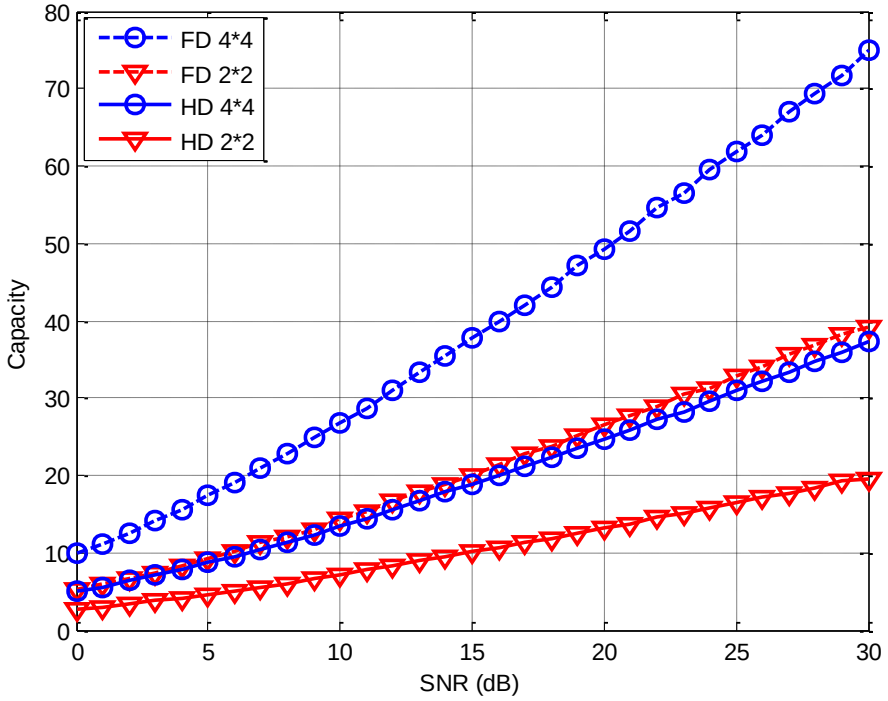

Figure 4.8. Capacity of full-duplex point-to-point MIMO system with perfect self-interference cancellation and those of the half-duplex MIMO system.

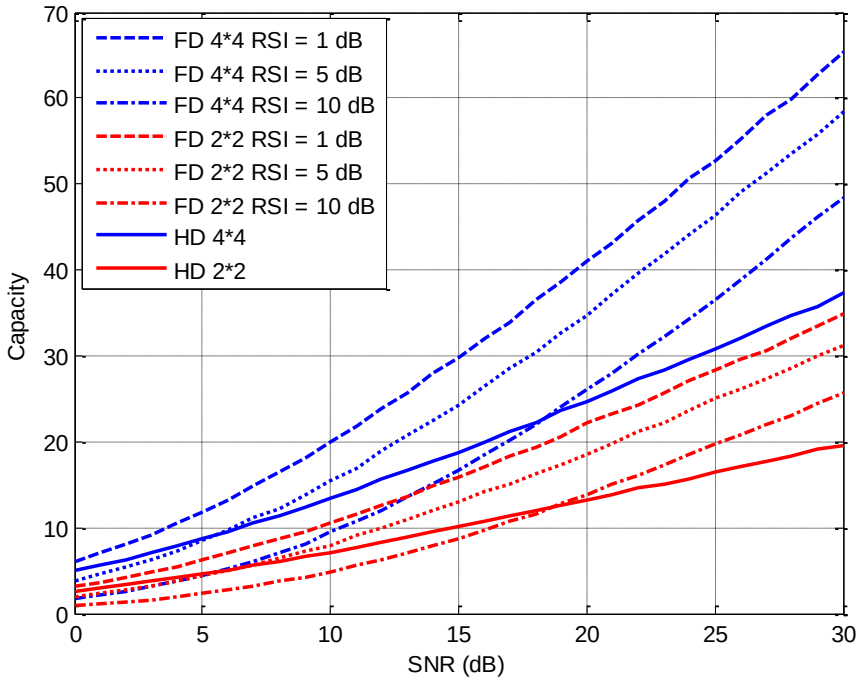

Figure 4.9. Capacity of full-duplex point-to-point MIMO system with imperfect self-interference cancellation and those of the half-duplex MIMO system.

4.6.2. Full-duplex MIMO Relay link

A relay link, a transmitter node (node 1), a decode-and-forward relay, and a receiver node (node 2) is shown in Fig. 4.10. The node 1 has N_1 and node 2 has N_2 channels (antennas) in half-duplex mode. The relay has total *N* channel, N_t channels for the transmission and N_r channels for the reception. The channels from node 1 to relay, from relay to note 2 and from relay to relay (self-interference) are denoted as $\mathbf{H}_{1R}$, $\mathbf{H}_{R2}$ and $\mathbf{H}_{RR}$, respectively. Let ρ_s and ρ_r are the average signal transmission power for note 1 and relay, respectively.

For the half-duplex operations, the received signal at the relay and note 2 can be written as:

$$\boldsymbol{y}_r = \sqrt{\rho_s}\,\mathbf{H}_{1R}\mathrm{x}_1 + \mathbf{n}_{r,} \tag{4.21}$$

$$\boldsymbol{y}_2 = \sqrt{\rho_r}\,\mathbf{H}_{R2}\mathrm{x}_r + \mathbf{n}_2.$$

The avarage SNR at the relay and node 2 can be obtained as

$$\gamma_r^{\mathrm{HD}} = \frac{\rho_s}{\sigma_r^2} \quad \text{and} \quad \gamma_2^{\mathrm{HD}} = \frac{\rho_r}{\sigma_2^2}. \tag{4.22}$$

Therefore, the average rate of relay and node 2 can be derived as

$$R_r^{\mathrm{HD}} = \mathrm{E}_{\mathbf{H}_{1R}}\left[\log_2\det\left(\mathbf{I} + \frac{\gamma_s^{\mathrm{HD}}}{N_1}\mathbf{H}_{1\mathrm{R}}^H\mathbf{H}_{1R}\right)\right],$$

$$R_2^{\mathrm{HD}} = \mathrm{E}_{\mathbf{H}_{R2}}\left[\log_2\det\left(\mathbf{I} + \frac{\gamma_2^{\mathrm{HD}}}{N_t}\mathbf{H}_{\mathrm{R2}}^H\mathbf{H}_{R2}\right)\right], \tag{4.23}$$

respectively. The capacity of half-duplex cooperative is:

$$R^{\mathrm{HD}} = \min(R_r^{\mathrm{HD}},\ R_2^{\mathrm{HD}}). \tag{4.24}$$

For the full-duplex relaying, the received signal at the relay and node 2 can be expressed as

$$\boldsymbol{y}_r = \sqrt{\rho_s}\,\mathbf{H}_{1R}\mathbf{x}_1 + \sqrt{\eta}\mathbf{H}_{\mathrm{RR}}\mathbf{x}_{\mathrm{r}} + \mathbf{n}_r, \tag{4.25}$$

$$\boldsymbol{y}_2 = \sqrt{\rho_r}\,\mathbf{H}_{R2}\mathbf{x}_r + \mathbf{n}_2.$$

The avarage SNR at the relay and node 2 can be obtained as

$$\gamma_r^{\mathrm{FD}} = \frac{\rho_s}{\eta+\sigma_r^2} \quad \text{and} \quad \gamma_2^{\mathrm{FD}} = \frac{\rho_r}{\sigma_2^2}. \tag{4.26}$$

Therefore, the average rate of relay and node 2 are derived by

$$R_r^{\mathrm{FD}} = \mathrm{E}_{\mathbf{H}_{1R}}\left[\log_2\det\left(\mathbf{I} + \frac{\gamma_r^{\mathrm{FD}}}{N_1}\mathbf{H}_{1\mathrm{R}}^H\mathbf{H}_{1R}\right)\right],$$

$$R_2^{\mathrm{FD}} = \mathrm{E}_{\mathbf{H}_{R2}}\left[\log_2\det\left(\mathbf{I} + \frac{\gamma_2^{\mathrm{FD}}}{N_t}\mathbf{H}_{\mathrm{R2}}^H\mathbf{H}_{R2}\right)\right], \tag{4.27}$$

respectively. Finally, the capacity of full-duplex cooperative is

$$R^{\mathrm{FD}} = \min(R_r^{\mathrm{FD}},\ R_2^{\mathrm{FD}}). \tag{4.28}$$

The half-duplex and full-duplex relay scenarios are simulated and the capacities are compared when the full-duplex relay can perfectly cancel its self-interference or when the self-interference cancellation is imperfect. Fig. 4.11 displays the simulation results for these capacities. It is observed that the link capacity using full-duplex ralay with perfect self-interference cancellation is twice as those with half-duplex relay. And Fig. 4.12 shows similar results this time with imperfect self-interference cancellation at the full-duplex relay. It is observed that the link capacity using full-duplex relay with perfect self-interference cancellation is twice as those with half-duplex relay. Moreover, it is observed that with an increase in the residual self-interference power in the full-duplex relay, the capacity of the link is decreased proportionally. Moreover, when the residual self-interference is large, the capacity of full-duplex is less than that of half-duplex, e.g. when the SNR is less 17 dB, the capacity of full-duplex at RSI = 10 dB is less than those of half-duplex.

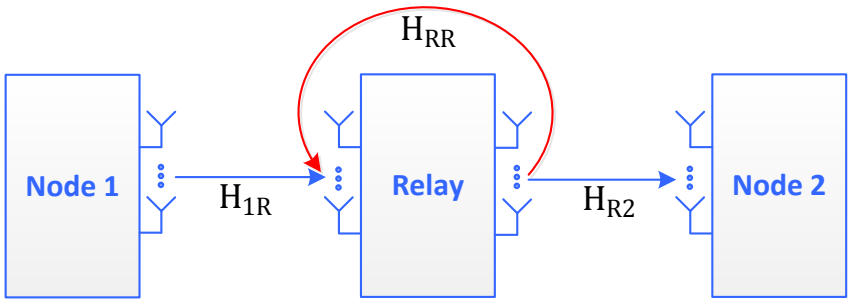

Figure 4.10. Block diagram of the full-duplex relay link.

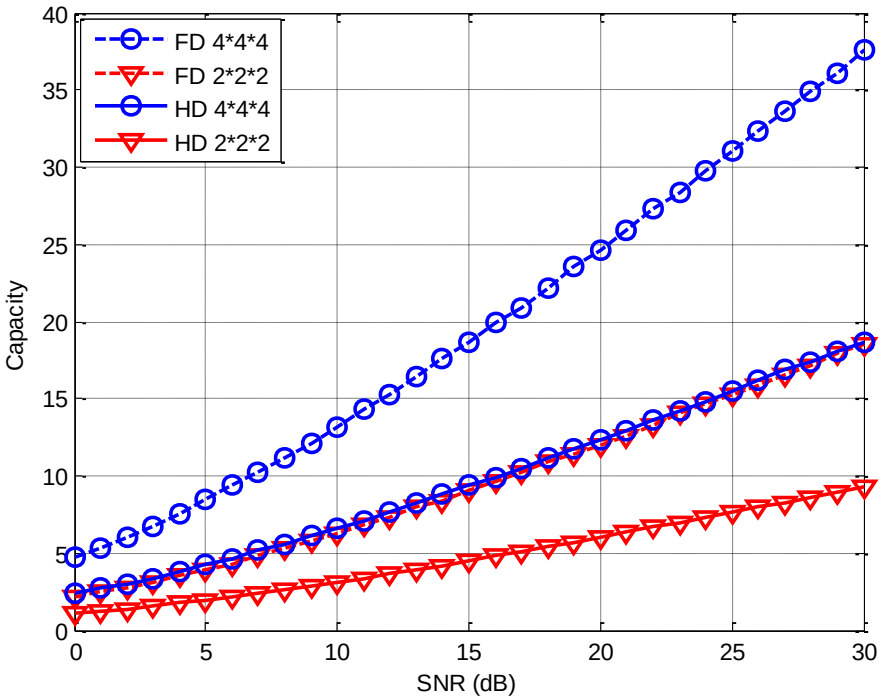

Figure 4.11. Capacity of full-duplex relay link with perfect self-interference cancellation and those of the half-duplex relay link.

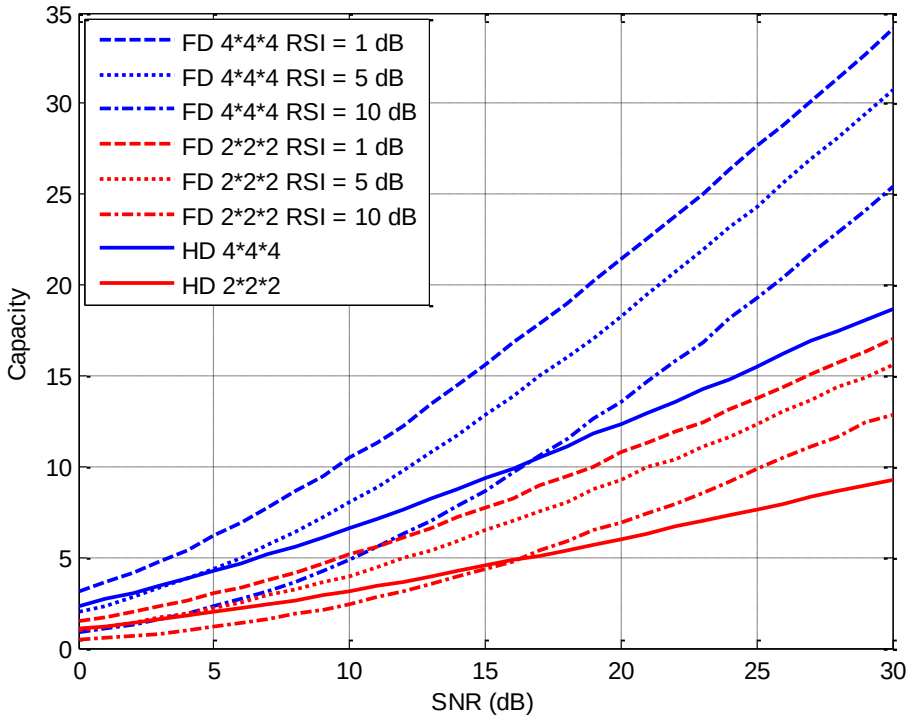

Figure 4.12. Capacity of full-duplex relay link with imperfect self-interference cancellation and those of the half-duplex relay link.

4.7. Summary

This section presents some analysis on the capacity of full-duplex MIMO systems, the digital self-interference cancellation, by using an estimate of the MIMO self-interference channel, as well as the capacity of point-to-point full-duplex MIMO and full-duplex MIMO relay links were investigated. Moreover, for the purpose of mitigating the residual self-interference, two precoding schemes, i.e. ZF and SLNR-based precoding, were analyzed and the performances were investigated. The simulation results indicate that when the self-interference channel estimation error is significant employing these precoding schemes help to improve the performance of the full-duplex MIMO system. In addition, the simulated sum-rate of the precoding schemes in the full-duplex MIMO system is almost 1.8 times higher than those of the half-duplex system. As a future direction to this work, optimal resource allocation can be considered.

5. Digital baseband solutions for full-duplex transceiver proof-of-concept

5.1. Motivation

The algorithms used in the DUPLO proof-of-concept for the self-interference cancellation at the digital baseband are discussed in this section. The DUPLO proof-of-concept is based on WARP board version 3 (WARPv3) which integrated a Xilinx FPGA with two RF chains [30], [31]. DUPLO proof-of-concept includes two solutions at antenna and RF isolation and active cancellation [13]. These solutions are connected on the WARPv3 platforms and required modifications on the WARP system has been performed to enable the platform to operate in full-duplex [13]. The baseband algorithms for self-interference cancellation are implemented on this platform to cancel out the remaining self-interference in the received signal at the baseband. To test these algorithms, a set of measurements with each DUPLO solution is performed and the received data to the baseband is measured to test the digital self-interference cancellations before implementing them on the platform. The algorithms and their performances using the measured data are discussed in this section.

5.2. Baseband self-interference cancellation algorithm

In an in-band full-duplex link the local node is communicating to a full-duplex, or two half-duplex, remote node(s). The local node transmit digital baseband signal, $x(t)$, includes modulated data in the data-transmit period and pilot symbols during the training period used for channel estimation. After passing through analog circuits and RF chain, the transmit signal is contaminated with the transmitter noise, $v_{\mathrm{t}}(t)$. Thus the signal at the transmit antenna could be expressed as $s(t) = x(t)_t + v_{\mathrm{t}}(t)$, where $x_t(t)$ is the upconverted transmit signal at the transmit antenna port. At the local node receive antenna port, the received signal is composed of self-interference plus received signal from the remote node, i.e. the desired signal. Assuming the desired signal is $d(t)$, and desired signal channel response and self-interference channel response at the receive antenna port indicated by $h_{\mathrm{des}}(t)$ and $h_{\mathrm{si}}(t)$, then the total received signal at the receive antenna port, $r(t)$, can be expressed as

$$r(t) = h_{\mathrm{des}}(t) * d(t) + h_{\mathrm{si}}(t) * s(t) + v_{\mathrm{r}}(t) \tag{5.1}$$

where * indicates convolution and $v_{\mathrm{r}}(t)$ is the white Gaussian noise. For the narrowband signal this can be presented in the frequency domain at each subcarrier k as

$$R[k] = H_{\mathrm{des}}[k]D[k] + H_{\mathrm{si}}[k]S[k] + V_{\mathrm{r}}[k] \tag{5.2}$$

where $H_{\mathrm{des}}[k]$ and $H_{\mathrm{si}}[k]$ indicate the desired signal channel and self-interference channel at subcarrier k , and $D[k]$, $S[k]$ and $R[k]$ are narrowband desired signal, self-interference and the received signal, and $V_{\mathrm{r}}[k]$ is the narrowband receiver noise all values at subcarrier k .

The baseband processing of the test cases, as well as the demonstrator developed in DUPLO WP5, is based on the WARPLab OFDM Reference Design developed at Rice University [30], [13]. The WARP v3 platform is used as the local and far node for the proof-of-concept [31]. Since these platforms are originally designed for half-duplex operation, the control system of the WARP platform was modified to allow simultaneous reception and transmission.

The transmit signal is an OFDM signal with 48 data and 4 pilot subcarriers and the CP length is 16. Data modulations used are BPSK and 16-QAM where pilot symbols are always BPSK modulated. The transmitted signal consists of two different parts, the preamble and the data payload. The preamble consists of short training sequence (STS) part and long training sequence (LTS) part. Length of the STS part is 480 samples and it is formed from 30 repetitions of 16 sample long sequence whereas the length of the LTS part is 160 samples and it consists of 2.5 repetitions of 64 samples sequence. Here STS is used to find the correct timing for self-interference cancellation and self-interference channel estimation.

A number of measurements were performed to evaluate the performance of digital and RF cancellation schemes. These measurements were performed with two full-duplex transceivers using different analog cancellation solutions. The first solution, Solution 1, is based on the usage of dual polarized antennas and active cancellation, whereas the second solution, Solution 2, is based on the use of electrical balance duplexer circuit [32]. The performances of the full-duplex self-interference cancellations, with and without digital self-interference solutions, are investigated. A set of measurement data is used to describe the analysis method and the algorithms used. Then the performance of the algorithms on all measurement data is presented in section 5.4.

5.3. Measurement data processing

A sample of the measurement data analysis is presented here with the data from measurement with the Solution 1. The signal transmitted is a 16-QAM modulated OFDM signal generated using the WARPLab OFDM Reference Design. Number of transmitted OFDM symbols is 190 and transmit power is 10 dBm (10 mW). The measurement data sets include 16,384 complex samples from the received signal. The real part of the received signal is shown in Fig. 5.1, where the end samples which are noise-only samples are represented in Fig. 5.2. As can be seen in Fig. 5.1 the received signal has a bias term (called DC-offset in the following). This DC-offset can be seen more clearly in Fig. 5.2 which shows signal samples 15,900 – 16,384. The SNR of the received signal is estimated from the samples as

$$SNR = 10 \cdot \log_{10}\left(\frac{P_{\text{rx,sig}}}{P_{\text{rx,noise}}} - 1 \right) \tag{5.3}$$

Where $P_{\text{rx,sig}}$ is the power calculated from the received self-interference signal and $P_{\text{rx,noise}}$ from noise-only samples. Two different $P_{\text{rx,noise}}$ values were calculated, one with DC offset and one without DC offset. In this case the SNR with DC-offset is 27.2 dB and without considering the DC offset 34.5 dB. Thus the DC-power-to-noise variance ratio in this case is 7.3 dB.

The spectrum of the received signal is shown in Fig. 5.3. The spectrum is calculated from the data modulated samples (sample numbers 2000 – 14,000). The nonuniform response of the analog/RF self-interference cancellation of the Solution 1 is clearly visible from the Fig. 5.3. Spectrum of the noise-only samples is shown in Fig. 5.4. This is calculated from samples 15,885 to 16,384. The eak at the center of the spectrum is the DC-offset but also other spurious signal components can be seen.

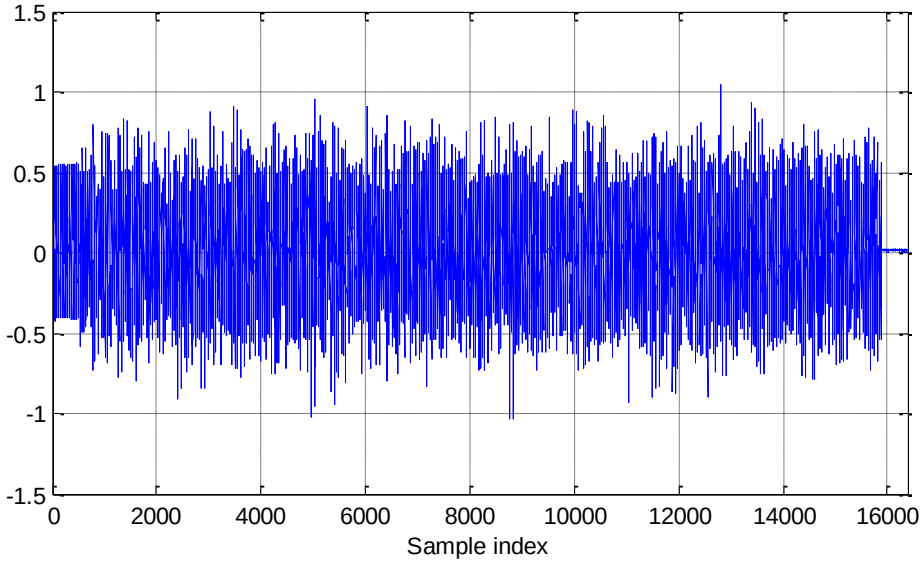

Fig. 5.1. Real part of the received signal.

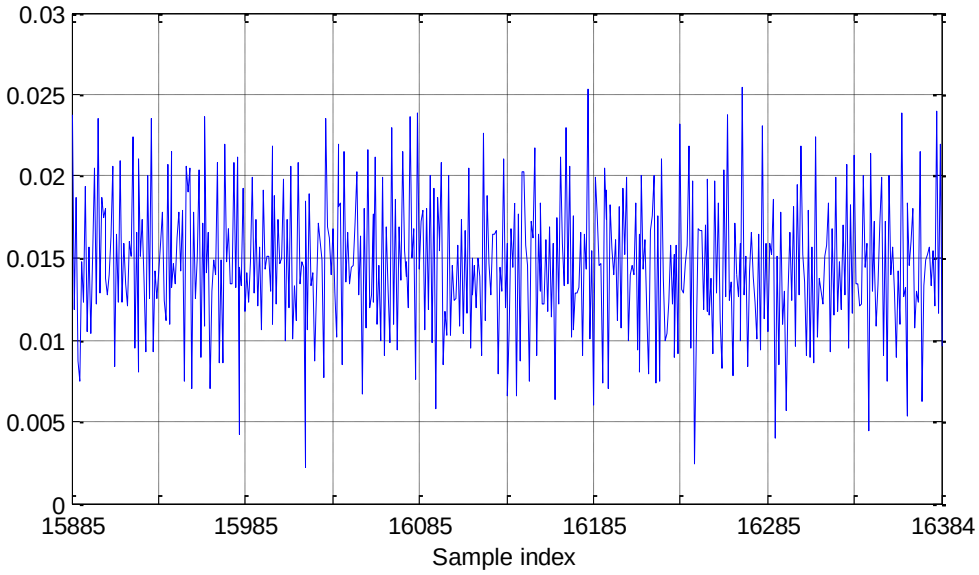

Fig. 5.2. Real part of the received noise-only samples.

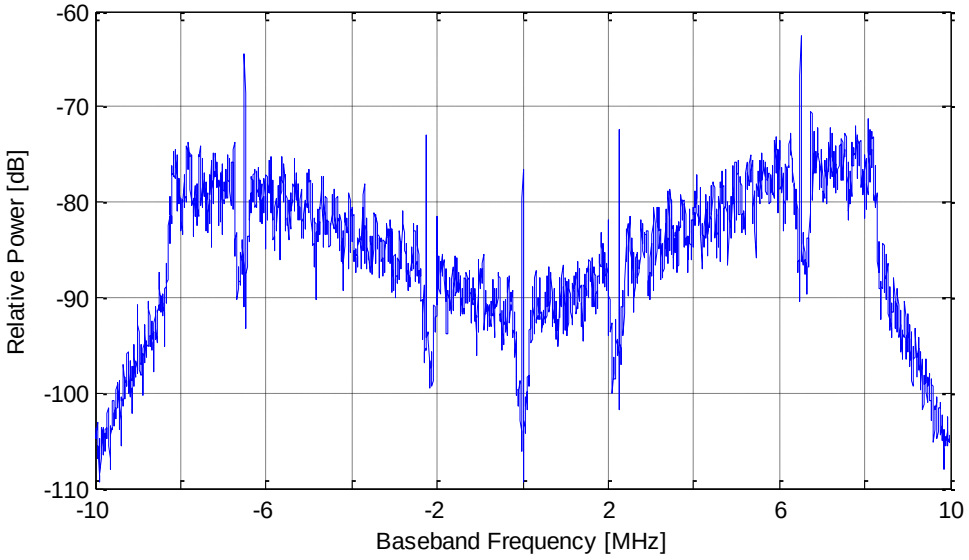

Fig. 5.3. Spectrum of the received signal (self-interference).

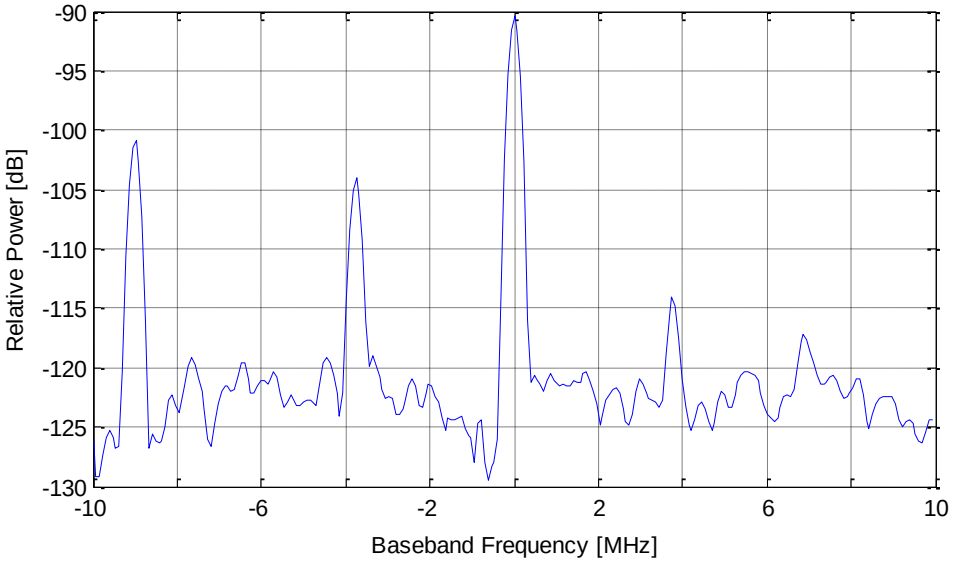

Fig. 5.4. Spectrum of the noise-only received samples.

5.3.1. Channel estimation

The channel is estimated in frequency domain using the channel estimator in the OFDM reference model. This estimator is commonly used and the channel estimates for subcarriers k is calculated as

$$\hat{h}_{\mathrm{si},k} = \frac{1}{2}\left(R_1[k] + R_2[k]\right) X^*[k] \tag{5.4}$$

Where $R_1[k]$ and $R_2[k]$ are received signal at subcarrier k from consecutive LTS sequences and $X[k]$ is the transmitted LTS symbol at subcarrier k. The channel estimate (absolute value and phase) is shown in Fig. 5.5.

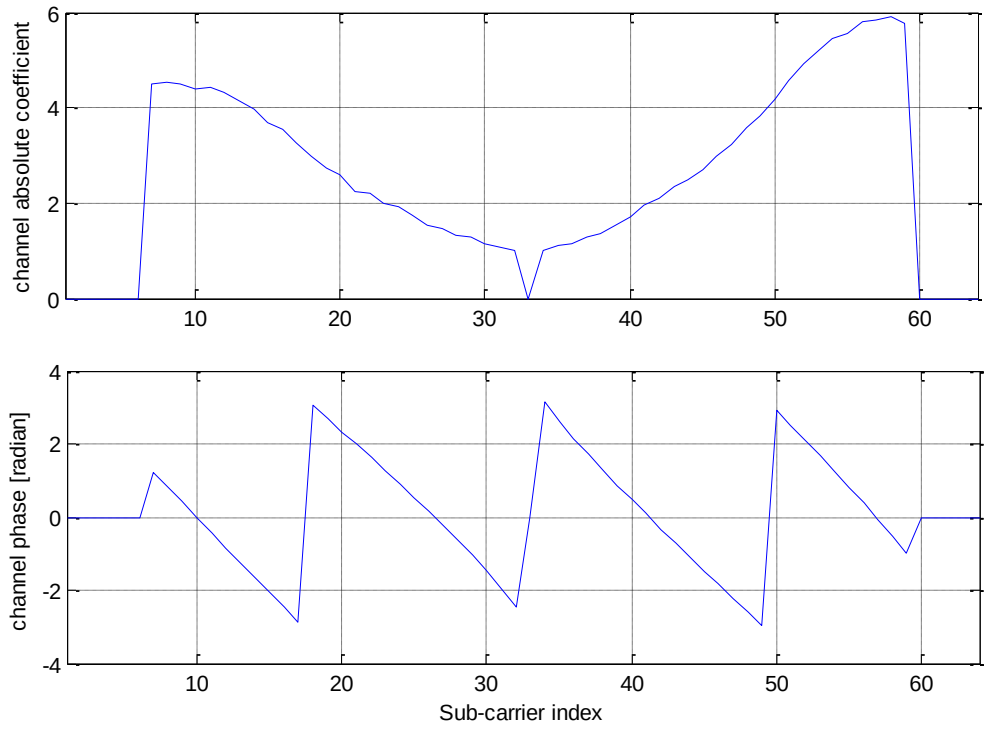

Fig. 5.5. SI channel estimate.

5.3.2. Frequency domain self-interference cancellation

When the signal received from the remote node and the self-interference are time aligned, i.e., OFDM symbol boundaries for the both signals are the same, the self-interference cancellation can be done in subcarrier domain without inter symbol interference. In this case, the known transmitted data symbols from the local node are multiplied by the self-interference channel estimate to emulate the received self-interference and then it is subtracted from the received signal. Fig. 2.6 shows one OFDM symbol in frequency domain before self-interference cancellation (red), emulated self-interference (black) and the received signal after self-interference cancellation (blue). It is observed that the average self-interference cancellation over 190 OFDM symbols is 28.4 dB.

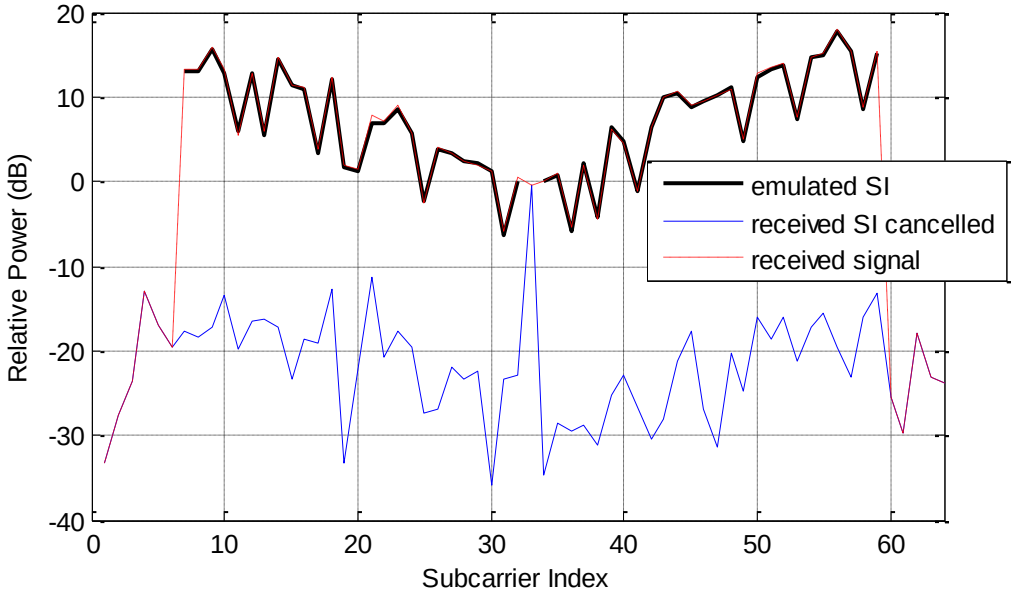

Fig. 5.6. SI cancellation at subcarrier domain.

5.3.3. Time domain self-interference cancellation

The time alignment of the received signal and self-interference cannot be always guaranteed in a practical system. This is also the case for the DUPLO demonstrator [13]. To overcome this, the self-interference cancellation can be done also in time domain. In this case the emulated self-interference is formed by convolving the known transmitted signal $x(t)$ with the estimated impulse $\hat{h}_{si}(t)$ response. The channel impulse response $\hat{h}_{si}(t)$ is calculated by taking the discrete inverse Fourier transform (IDFT) of the frequency domain channel estimate Eq. (5.4). After interference cancellation received signal $y(t)$ is

$$y(t) = r(t) - \hat{h}_{si}(t) * x(t) - \bar{r}(t) \tag{5.5}$$

where the received signal $r(t)$ is presented with Eq. (5.1) and $\bar{r}(t)$ is time average of the received signal which is used to remove the DC-offset. The spectrum of the received signal before and after the time domain cancellation is shown in Fig. 5.7. The cancellation performance calculated directly from the time domain signal in this case is 19.8 dB. When calculating the self-interference cancellation performance at data subcarriers the self-interference cancellation performance averaged over 190 symbols is 23.0 dB. As can be seen from the Fig. 5.7 the cancellation at the band edges and near the center frequency is lower than at other parts of the spectrum. When disregarding subcarriers at the band edges (subcarriers 7 and 59) and around center frequency (subcarriers 32 and 34) and calculating the self-interference performance at subcarriers 35–58 the self-interference performance is 25.5 dB and at subcarriers 8–31 the self-interference cancellation performance is 24.4 dB.[2]

Frequency domain channel estimation is done at subcarriers according to Eq. (5.4). In effect this corresponds to the case when the frequency response of the channel is multiplied with a rectangular window. When IDFT of the frequency response is calculated to get the channel impulse response this rectangular windowing can decrease time domain self-interference

[2] No transmission at subcarriers 1 – 7 and 59 – 64 (guard bands) nor 33 (center frequency). See Fig. 5.9 for sub-carrier indices.

cancellation performance. In order to improve the performance of the time domain cancelation Hamming and Hanning windowing of the impulse response were tested. Hamming window is defined as [33]

$$w_{\text{Hamming}}(n) = 0.54 - 0.46 \cdot \cos\left(\frac{2\pi n}{M-1}\right) \tag{5.6}$$

and Hanning window as [33]

$$w_{\text{Hanning}}(n) = \frac{1}{2}\left(1 - \cos\frac{2\pi n}{M-1}\right) \tag{5.7}$$

Table 5.1 presents the self-interference cancellation values when Hamming and Hanning windowing is used. As can be seen the self-interference cancellation averaged over all the subcarriers is better when no windowing but performance at subcarriers 35–58 and 8–31 windowing increases the performance about 2 dB with both windowing functions.

Table 5.1. Time domain self-interference cancellation with windowing in the self-interference channel estimation

	Hamming	Hanning
SIC: time domain (data subcarriers)	19.9	20.1 dB
SIC: time domain (subcarriers 35-58)	27.9	27.9 dB
SIC: time domain (subcarriers 8-31)	26.5	26.5 dB

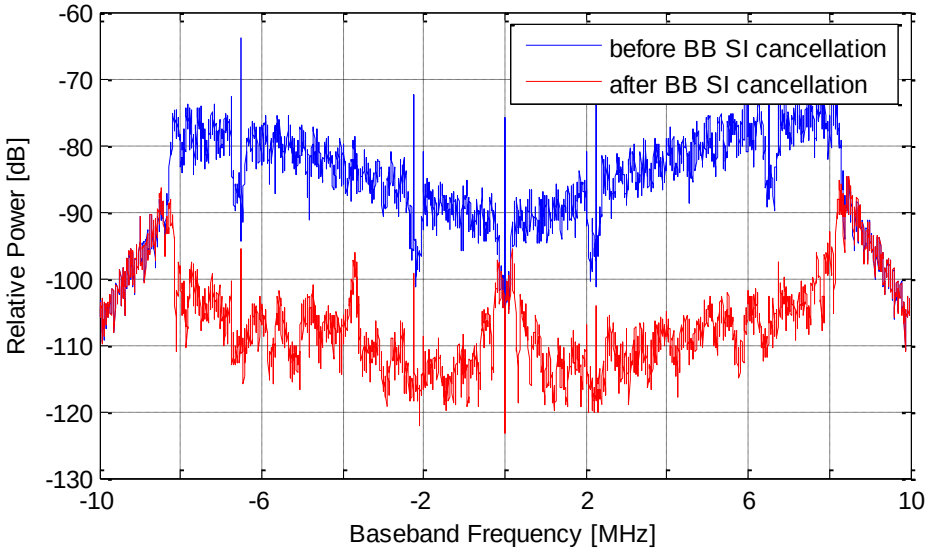

Fig. 5.7. Self-interference spectrum before and after time-domain self-interference cancelation.

5.3.4. LMS based self-interference cancellation

In the analysis presented above the self-interference channel is estimated using the LTS, i.e., the channel estimate is calculated using two 64 samples training sequence. The self-interference channel can also be estimated using adaptive filtering techniques. For instance the LMS algorithm is a simple adaptive algorithm that allows more data samples to be used in the self-interference channel estimation. In this approach, channel taps are the LMS filter coefficients, $\mathbf{w}_n$, and the input signal is the training signal, $\mathbf{u}_n$, the channel coefficients' updates are calculated as [34]

$$\mathbf{w}_{n+1} = \mathbf{w}_n + \mu \mathbf{u}_n e_n^*, \tag{5.7}$$

where μ the step size used for the coefficients update and e_n is the estimation error.

After the channel is estimated using LMS algorithm, self-interference cancellation is done in time domain. Figure 5.8 shows the spectrum before (blue curve) and after LMS based cancellation (red curve) when 26 OFDM symbols are used for self-interference channel estimation and the filter lengh is 54. The number of OFDM symbols in Fig. 5.8 was was selected so that the LMS based cancellation gives about the same cancellation performance (i.e. 28.7 dB) compared to the subcarrier domain cancellation (i.e. 28.4 dB). When all the 190 OFDM symbols are used for self-interference cancellation, an average self-interference cancellation of 30 dB can be achieved.

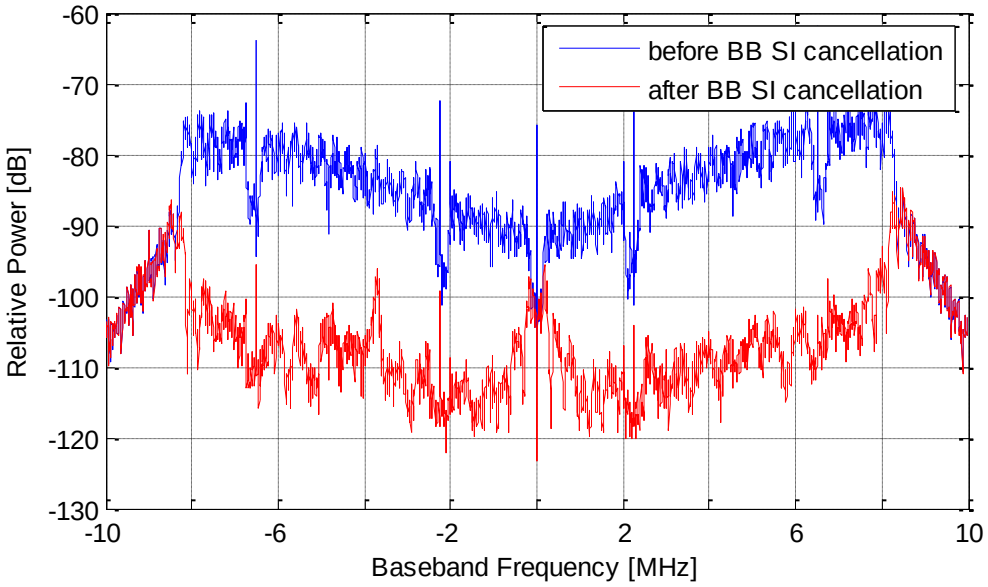

Fig.5.8. Self-interference spectrum before and after self-interference cancellation using the LMS algorithm for self-interference channel estimation with time-domain cancellation.

5.4. Summary and discussion of results

Figure 5.9 summarizes the self-interference any digital baseband self-interference cancellation and after subcarrier domain, time domain and LMS based self-interference cancellation for the sample measurement data. The values are averaged over 190 OFDM symbols.

Measured data Solution 1 at transmit powers 0 dBm, 10 dBm and 15 dBm with 16-QAM and BPSK modulations were used in the analysis of digital baseband self-interference cancellation. Table 5.2 and 5.3 show the baseband self-interference cancellation values for these cases. Four data sets from measurements with the Solution2 have also been analyzed. These measurements are from a setup with BPSK modulation and -6 dBm transmit power. Table 5.4 gives baseband cancellation values for these cases. The signal structure in the measurements with the Solution 2 has been the same as with the Solution 1 except the signal length. The data payload length with the Solution 2 tests has been 40 OFDM symbols (190 in TTI data). Values presented in Tables 5.2, 5.3 and 5.4 are calculated as explained in the example case presented above. Hanning window is used in time domain self-interference cancellation in these cases.

The purpose of the analysis presented here is to provide baseband self-interference solution for the DUPLO full-duplex demonstrator development, which is worked out in DUPLO WP5. All the cases here are from a single node setups, i.e., the received signal contains only the self-interference and possible spurious signals from the environment or generated inside the equipment. The plot of the noise spectrum in Fig 5.4 shows that there are some spurious signal summing up to the received signal. Also the averaged self-interference cancellation at different subcarriers in Fig. 5.9 indicates that there is an underlying interfering signal at subcarrier 21. The data sample set for calculating the spectrum in Fig 5.4 is quite small but spurious components are present in all the data sets, they can be seen also in tests not reported here. Although it is possible that some of the spurious signals are received from the environment they are most probably generated in the WARP platform itself. These spurious signals can be pushed below noise level by changing the gain values but this would also decrease the dynamic range of the

receiver. The value of the DC offset is also present in all the cases. The observation is that the performance of the baseband self-interference cancellation is mainly affected by the DC offset compared to other factors such as nonlinear effects discussed in Chapter 2.

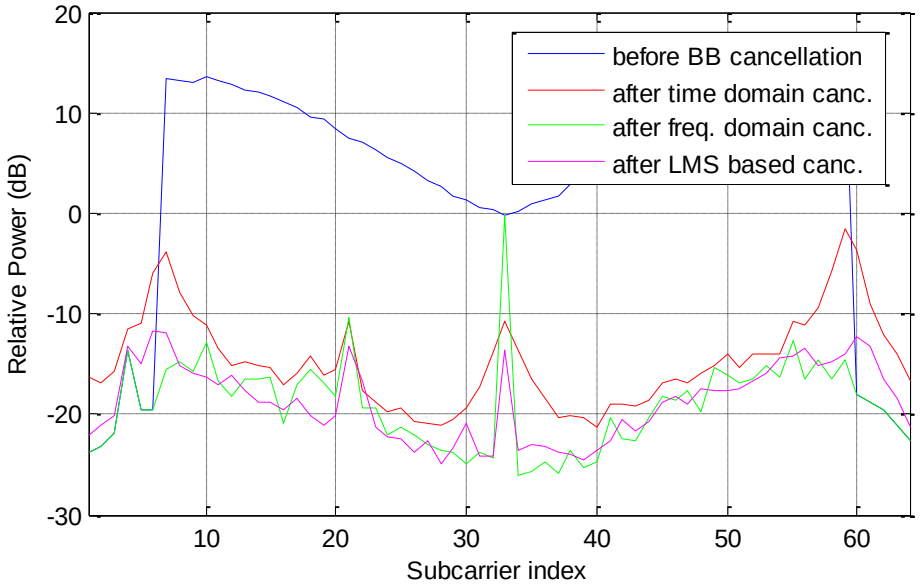

Fig. 5.9. Average SI cancellation per subcarrier.

Table 5.2. Solution 1 data sets, 16-QAM data modulation.

TX power	0 dBm	10 dBm	15 dBm
SNR with DC	17.2 dB	27.2 dB	33.7 dB
SNR without DC	25.0 dB	34.5 dB	41.2 dB
DC power/noise variance	7.7 dB	7.3 dB	7.4 dB
SIC: freq. domain	25.5 dB	28.4 dB	28.2 dB
SIC: time domain	18.9 dB	19.1 dB	18.7 dB
SIC: time domain (data subcarriers)	20.2 dB	20.1 dB	20.1 dB
SIC: time domain (subcarriers 35-58)	27.3 dB	27.9 dB	27.7 dB
SIC: time domain (subcarriers 8-31)	24.0 dB	26.5 dB	26.0 dB
SIC: LMS based (whole signal)	26.2 dB	30.0 dB	29.8 dB

SIC: LMS based (2600 samples)	25.5 dB	28.4 dB	27.8 dB

Table 5.3. Solution 1 data sets, BPSK data modulation.

TX power	0 dBm	10 dBm	15 dBm
SNR with DC	17.6 dB	29.8 dB	34.4 dB
SNR without DC	25.4 dB	37.9 dB	43.3 dB
DC power/noise variance	7.8 dB	8.1 dB	9.1 dB
SIC: freq. domain	24.2 dB	22.6 dB	26.7 dB
SIC: time domain	18.7 dB	20.2 dB	19.9 dB
SIC: time domain (data subcarriers)	19.5 dB	19.5 dB	20.7 dB
SIC: time domain (subcarriers 35-58)	26.9 dB	24.7 dB	26.8 dB
SIC: time domain (subcarriers 8-31)	21.6 dB	21.0 dB	25.7 dB
SIC: LMS based (whole signal)	25.0 dB	21.4 dB	26.6 dB
SIC: LMS based (2600 samples)	23.3 dB	21.8 dB	26.1 dB

Table 5.4. Solution 2 data sets, BPSK data modulation, TX power -6 dBm.

Data set number	001	002	003	004
SNR with DC	2.6 dB	2.5 dB	2.4 dB	2.5 dB
SNR without DC	14.1 dB	14.0 dB	13.3 dB	13.7 dB
DC power/noise variance	12.0 dB	11.8 dB	11.4 dB	11.9 dB
SIC: freq. domain	13.3 dB	13.0 dB	12.7 dB	12.8 dB
SIC: time domain	15.2 dB	15.2 dB	14.7 dB	14.8 dB
SIC: time domain (data subcarriers)	12.7 dB	12.8 dB	12.1 dB	12.5 dB

SIC: time domain (subcarriers 35-58)	15.1 dB	15.4 dB	14.8 dB	15.2 dB
SIC: time domain (subcarriers 8-31)	11.6 dB	11.4 dB	10.6 dB	10.6 dB
SIC: LMS based (whole signal)	13.3 dB	13.2 dB	12.4 dB	13.3 dB
SIC: LMS based (2600 samples)	13.4 dB	13.2 dB	12.6 dB	13.1 dB

6. Summary

This document presented some results on the analysis and simulation of digital baseband solutions for full-duplex transceiver, i.e. full-duplex transceiver self-interference cancellation.

Specifically, since the transmitter PA has been identified as a main source of nonlinear components in the full-duplex systems' self-interference, the modelling, simulation and evaluation of the effect of PA on the performance of a full-duplex system is presented. In this regard, three different methods in the analysis of the problem is presented and performances are compared.

Moreover different detection methods, namely zero-forcing, maximum likelihood and minimum mean square method, are analysed and the performances are comparatively evaluated through simulations. Simple multiple-access techniques in a multiuser full-duplex scenario are investigated as well.

Since MIMO is one of the most important techniques in the current wireless systems, full-duplex needs to coexist with this technology, but a main challenge for full-duplex MIMO systems is how to cancel self-interference from multiple collocated transmit antenna concurrently, while preventing the LNA and ADC of the receive chain from saturation. At the digital baseband however smart precoding techniques can help in reducing the self-interference while maximizing the transmitted signal in the direction of the remote receiver. A couple of precoding techniques investigated to be used concurrently with the digital self-interference cancellation to reduce the amount of residual self-interference cancellation. These investigations shows that the employed precoding schemes, i.e. ZF and SLNR-based, can significantly improve the performance of a full-duplex MIMO system. On the other hand, achievable capacities in a point-to-point full-duplex MIMO link and a full-duplex MIMO relay link are investigated and compared to the half-duplex capacities. Results show that the full-duplex gain is achieved conditioned on a very good self-interference cancellation performance.

Finally, as input to the DUPLO proof-of-concept, practical digital self-interference cancellation algorithms are implemented which works in cooperation with antenna, isolation circuits and active RF cancellation circuits to provide the full proof-of-concept for the DUPLO solutions. To analyze the practical achievable performance of the digital baseband solutions, measurement data from a number of tests with the antenna and RF solutions implemented in DUPLO WP2 was performed. These analyses presented in this document shows that the self-interference cancellation in time-domain is preferable since the accurate synchronization which is required for the frequency-domain self-interference cancellation might not be always practical. The best achievable digital baseband self-interference cancellation using the solutions presented in this report is close to 30 dB. Moreover it was observed that DC-offset is a main component in reducing the performance of self-interference cancellation at the digital baseband.

7. References

[1] Mir Ghoraishi, 'Digital Baseband Solutions for Full-Duplex Transceiver,' INFSO-ICT- 316369 DUPLO - Report D3.1, April 2014.

[2] V. Tapio, "System scenarios and technical requirements for full-duplex concept", INFSO-ICT-316369 DUPLO - Report D1.1, April 2013.

[3] D. Bharadia, E. McMilin, and S. Katti, "Full duplex radios," in Proc. SIGCOMM'13, Aug. 2013, pp. 375–386.

[4] V. Syrjala, M. Valkama, L. Anttila, T. Riihonen, D. Korpi, "Analysis of Oscillator Phase-Noise Effects on Self-Interference Cancellation in Full-Duplex OFDM Radio Transceivers," IEEE Trans. on Wireless Communications, Vol. 13, No. 6, pp. 2977 - 2990, 2014.

[5] A. Sahai, G. Patel, C. Dick, A. Sabharwal, "On the Impact of Phase Noise on Active Cancelation in Wireless Full-Duplex," IEEE Trans. on Vehicular Technology, Vol. 62, No. 9, pp. 4494 - 4510, 2013.

[6] D. Korpi, L. Anttila, V. Syrjala, M. Valkama, "Widely Linear Digital Self-Interference Cancellation in Direct-Conversion Full-Duplex Transceiver," IEEE Journal on Selected Areas in Communications, Vol. 32, No. 9, pp. 1674-1687, 2014.

[7] D. Korpi, T. Riihonen, V. Syrjala, L. Anttila, M. Valkama, R. Wichman, "Full-Duplex Transceiver System Calculations: Analysis of ADC and Linearity Challenges," IEEE Trans. on Wireless Communications, Vol. 13, No. 7, pp. 3821-3836, 2014.

[8] Anttila, L.; Korpi, D.; Syrjala, V.; Valkama, M., "Cancellation of power amplifier induced nonlinear self-interference in full-duplex transceivers," *Signals, Systems and Computers, 2013 Asilomar Conference on*, 3-6 Nov. 2013.

[9] J. Mietzner, R. Schober, L. Lampe, W. Gerstacker, P. Hoeher, "Multiple-antenna techniques for wireless communications - a comprehensive literature survey," IEEE Communications Surveys Tutorials, vol. 11, no. 2, pp. 87–105, June 2009.

[10] B. Day, A. Margetts, D. Bliss, P. Schniter, "Full-Duplex Bidirectional MIMO: Achievable Rates Under Limited Dynamic Range," IEEE Trans. on Signal Processing, Vol. 60, No. 7, July 2012.

[11] E. Aryafar, M. A. Khojastepour, K. Sundaresan, S. Rangarajan, and M. Chiang, "Midu: enabling MIMO full-duplex", 18th annual international conference on Mobile computing and networking, Mobicom '12, pages 257–268, New York, NY, USA, 2012. ACM.

[12] D. Bharadia, S. Katti, "Full Duplex MIMO Radios," SIGCOM, 2013.

[13] C. Lavin, "Final proof-of-concept validation, results and analysisEarly integration and test", INFSO-ICT- 316369 DUPLO - Report D5.2, May 2015.

[16] B. Debaillie, "Integration report of RF and antenna self-interference cancellation techniques", INFSO-ICT- 316369 DUPLO - Report D2.2, October 2014.

[17] B. Debaillie, et al., "Analog/RF Solutions Enabling Compact Full-Duplex Radios," *Selected Areas in Communications, IEEE Journal on*, vol.32, no.9, pp.1662,1673, Sept. 2014.

[UO2] H. Alves, et al., "On the Average Spectral Efficiency of Interference-Limited Full-Duplex Networks", *Cognitive Radio Oriented Wireless Networks and Communications (CROWNCOM), 2014 9th International Conference on,* 2-4 June 2014.

[14] D. Schreurs, M. O'Droma, A.A. Goacher, M. Gadringer (Ed.), *RF Power Amplifier Behavioral Modeling*, Cambridge University Press. 2009.

[18] *Part 11: Wireless LAN Medium Access Control (MAC) and Physical Layer (PHY) Specifications*, IEEE Std 802.11-2012.

[19] J. Heiskala, J. Terry, *OFDM Wireless LANs: A Theoretical and Practical Guide*, Sams Publishing, 2002.

[20] R. V. Nee and R. Prasad, "OFDM for Wireless Multimedia Communications", *Artech House*, 2000.

[21] H. G. Myung, J. Lim, and D. J. Goodman, "Single Carrier FDMA for Uplink Wireless Transmission", *IEEE Vehicular Technology Magazine*, vol. 1, no. 3, pp. 30-38, Sep. 2006.

[G3] C. Xiao, Y. Zheng, N. C. Beaulieu., "Novel Sum-of-Sinusoids Simulation Models for Rayleigh and Rician Fading Channels", *IEEE Trans. Wireless Communication*, vol. 5, no. 12, pp.3667-3679, Dec. 2006.

[22] J. G. Proakis. Digital Communications. McGraw-Hill, third edition, 1995.

[23] Z. Xie, R. Short, and C. Rushforth, "A family of suboptimum detectors for coherent multiuser communications," *IEEE J. Select. Areas Commun.*, vol. 8, no. 4, pp. 683-690, May 1990.

[24] Yong Soo Cho, Jaekwon Kim, Won Young Yang, Chung G. Kang, "MIMO-OFDM Wireless Communications with MATLAB", *John Wiley & Sons (Asia) Pte Ltd*., 2010.

[25] M. Sadek, A. Tarighat, and A. H. Sayed, "A leakage-based precoding scheme for downlink multi-user MIMO channels," IEEE Transactions on Wireless Communications, vol. 6, no. 5, pp. 1711–1721, May 2007.

[26] P. Xiao, M. Sellathurai, "Improved linear transmit processing for single-user and multi-user MIMO communications systems," IEEE Transactions on Signal Processing, vol. 58, no. 3, pp. 1768–1779, March 2010.

[27] A. Tarighat, M. Sadek, and A. H. Sayed, "A multi user beamforming scheme for downlink MIMO channels based on maximizing signal-to-leakage ratios," in Proc. IEEE Int. Conf. Acoust., Speech, Signal Process., Philadelphia, PA, Mar. 2005, vol. 3, pp. 1129–1132.

[28] G. Golub and C. V. Loan, "Matrix Computations", 3rd ed. Baltimore, MD: The Johns Hopkins Univ. Press, 1996.

[29] D. Tse, P. Viswanath, "Fundamentals of Wireless Communication", Cambridge University Press, 2005.

[30] https://warpproject.org/trac

[31] http://mangocomm.com/products/kits/warp-v3-kit

[32] B. van Liempd, C. Lavin, S. Malotaux, D. van den Broek, B. Debaillie, C. Palacios, J. Long, E. Klumperink, J. Craninckx, "RF Self-Interference Cancellation for Full-Duplex," Crowncom 2014, June 2014.

[33] J. G. Proakis, D. G., Manolakis, *Digital Signal Processing, Principles, Algortihms, and Applications, 3rd ed.*, Prentice-Hall, Inc., 1996.

[34] S. Hayking, *Adaptive Filter Theory, 3rd ed.*, Prentice-Hall, Inc., 2009.

[35] B. O'Hara, A. Petrick, *IEEE 802.11 Handbook: A Designer's Companion, Chapter 16: System design considerations for IEEE 802.11 WLANs*, John Wiley & Sons, 2nd Edition, 2011.